UCLouvain

École polytechnique de Louvain

Multiphase computational fluid dynamics for subsea jet trenching applications

Author: **Juliette KRUG**
Supervisors: **Matthieu CONSTANT, Jonathan LAMBRECHTS, Vincent LEGAT**
Reader: **Sandra SOARES-FRAZAO**
Academic year 2021–2022
Master [120] in Mechanical Engineering

Acknowledgments

I would like to express my thanks and my sincere gratitude to my supervisors, Dr. Matthieu Constant, Dr. Jonathan Lambrechts and Prof. Vincent Legat, who have helped, supported and guided me throughout this thesis. With meetings every two weeks, they have helped me move forward in the project and guided me when I did not know which direction to take. I am grateful for their words of motivation, their precious feedbacks and for ending every meeting on a positive remark, which I think is very important to keep a positive attitude during a long project. I especially want to thank Dr. Jonathan Lambrechts for his help with the debugging of the code and the coding itself.

I would also like to thank the other participants of those meetings, the Migflow team, Nathan Coppin and Michel Henry, and the other students writing their thesis, Leïla Schneidesch, Marie-Ombeline Wilmet, Manon Wouters and Simon Yans. Their patience, their support and their insights were always very much appreciated.

Finally, I would like to thank my family and friends for their constant support and words of encouragements. I would like to give my special thanks to Aaron, Adeline, Elisabeth and Roxane for their thoughtful attentions and for believing in me, as well as in this thesis.

Abstract

Subsea jet trenching is used to create trenches and bury cable in the sea floor, to bring electricity from offshore wind farms to the continent, for example. This is a preliminary study to determine if jet trenching can be modelled numerically and give accurate results. This is done using the software Migflow that solves immersed granular flows, and the results are compared to the laboratory experiments done by A.T.H. Perng and H. Capart [1], where a small vehicle uses jets to create a trench in a tank.

The Navier-Stokes equations and the incompressibility hypothesis are already implemented in the software. To those equations is added the concentration equation, that gives the evolution of the concentration of water with time. That equation is the sum of an advection equation and a mass diffusion equation. The sedimentation velocity, velocity at which the sand settles on the sea floor, is also determined, tested and added to the concentration equation.

This software, modified with the new equations, is tested on the setup done by Perng and Capart. The tests are first done to determine the impact on the simulations of the viscosity of the sand, the coefficient of sedimentation, the mass diffusion coefficient and the height of the jet. Finally, the velocity of the vehicle is analysed and compared to the laboratory results. The flux at the jet is also tested.

The conclusions are that the current model do not recreate the results of the experiments. Indeed, the results obtained when changing the velocity of the vehicle do not match the ones obtained in the laboratory. This is due to the dependence of the solution to the time step and to the use of the wrong model for the viscosity of the sand. This last problem could be solved modelling the sand as a non-Newtonian fluid. Despite the results to be improved, the concentration equations and the sedimentation velocity are both validated and implemented correctly in the software.

Contents

Chapter 1

Introduction

Subsea pipelines were introduced and built due to the emerging offshore petroleum industry in the middle of the 20th century [2]. They were and are still used for the offshore transport of crude oil and natural gas. Nowadays, the development of offshore wind farms requires the transport of electricity from the farm to the continent, and thus requires cables going through the oceans. To protect those cables from the elements and from anchors, they must be buried under a certain layer of sediment, in the sea floor. Due to those different applications, underwater trenching, also called dredging, to bury cables under a thick layer of sediment has been evolving and different methods have emerged [1].

The European Dredging Association defines two main categories of dredging, known as mechanical and hydraulic dredging [3]. One common component to all mechanical dredgers is a bucket to collect the soil and bring it to the surface, whereas hydraulic dredgers fluidize the material with the help of a pipe system and a centrifugal pump. Since the principle of hydraulic dredgers is based on the sediment going in suspension, it is most effective when the soil is made of very fine particles. Suction through the pipe system can be sufficient for loose materials and jets are incorporated to the device if the soil is too strong, to erode the sediment.

Mechanical dredgers are divided into different subcategories [3]. A first example is the bucket dredger, a stationary dredger containing an endless chain of buckets. Those buckets dig the sea floor and bring the material to the surface, releasing it into big barges on the boat. Another type of mechanical dredgers is the grab dredger. It is constituted of a grab, made of two half-shells controlled electrically or hydraulically. A final example is the backhoe dredger. It operates hydraulically and is made of one shell, that digs while moving towards the dredger.

This thesis is focused on hydraulic dredging, and several examples of such dredgers can be given. A first example is the suction dredger [3] [4], where the sediment is sucked in by a device connected to a stationary ship, leaving the trenches open. It is mainly used to mine for sand. A second example is the water injection dredger [5] and is made of a jetting system, where high pressure water is ejected from the device, setting the sediment in suspension. The trenches are closed once the sediment has fallen back due to the action of gravity. A last example is a dredger that includes a Remotely Operated Vehicle, ROV. Those exist in various designs and can be adapted depending on the application, the soil composition, the trench depth needed, etc. A good example of hydraulic dredger with ROV and jetting system is given on the website of the Global Offshore company [6]: the Q1400 Trenching ROV. It is used to bury flexible cables. It exists with two modes: chain cutting, figures 1.1a and 1.1b, or jetting, figures 1.1c and 1.1d.

The chain cutter mode is made of a chain that digs soils of up to 250 [kPa] but it needs a soil capable of bearing at least 12 [kPa]. The maximum diameter of the flexible product, cable for example, to be buried in the ground is 275 [mm]. It digs trenches of up to 2 [m] depth.

(a) ROV with chain cutting mode [6]

(b) Chain system

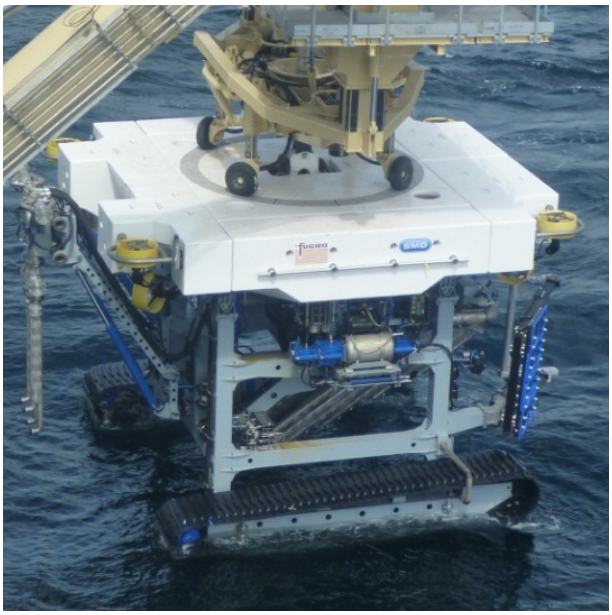

(c) ROV with jetting mode

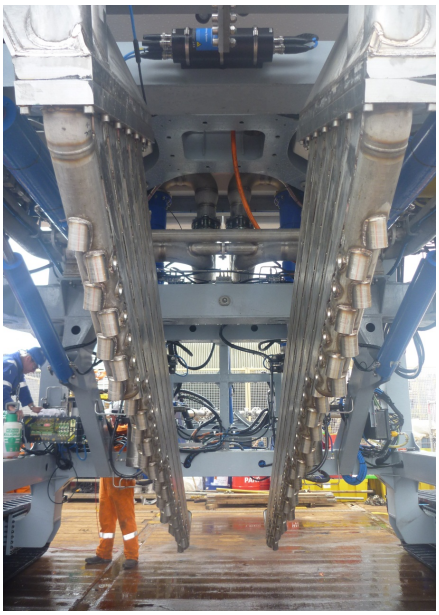

(d) Jetting system

Figure 1.1: The two models of the Q1400 Trenching ROV [7]

The jetter mode is made of a jetting tool that sends high pressure water towards the ground. It is the most efficient method for soils of up to 100 [kPa] [8] and needs a soil capable of bearing at least 5 [kPa]. It operates at depths of up to 1500 [m]. The maximum diameter of the product to be buried in the ground is 900 [mm]. The trenches can reach a depth of maximum 3 [m]. All the data has been retrieved from the ROV data sheet, found on the website of the Global Offshore company [6]. This jetting mode is the most interesting one in this case, and the study of this thesis is based on its working principle.

The Q1400 Trenching ROV with the jetter mode is a good example to explain the functioning of a jetting system. It is made of two spades, and the cable to be buried is placed in between those spades, in the space dedicated to that cable and shown on figure 1.1d. A simplified version of the jetting process is drawn on figure 1.2. The different steps are the following ones: the ROV is brought to the sea floor, with the spades horizontal. Then, the vertical high pressure jets on the spades are activated. Thanks to that, the soil is eroded and the spades can rotate up to their final predetermined angle, while the vehicle moves at constant velocity. The jets induce the erosion of the surface, the soil is fluidized and sedimentation takes place downstream of the jetting tool. At the back of the ROV are also high volume and low pressure jets, to maintain the non cohesive soil in suspension. The cable, controlled by a device in between the spades, has then time to sink in that fluidized mixture before the trench backfills. Indeed, due to gravity and depending on the flexibility of the cable, it sinks at a certain depth and is then covered by the soil, that settled as a result of the force of gravity acting on each of its particles. At the end of the process, the cable is released and buried underneath the sea floor and the ROV is brought back to the surface.

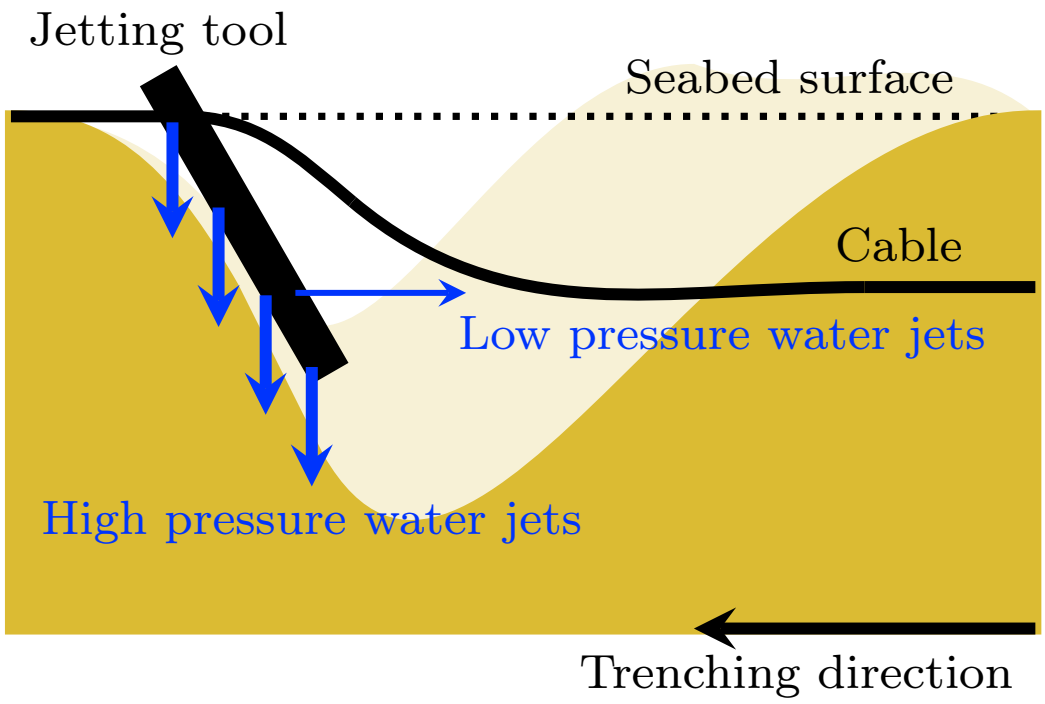

Figure 1.2: Simplification of the jetting technique (Adapted from [8])

The breaking process of the soil is different depending on the areas [8]:

- The cutting area, upstream of the ROV: the soil, first undisturbed, is eroded by the high pressure jets of water coming from the spades.
- The crushing area, in between the spades: the jetting tool is made of two spades separated by a certain distance. That distance is related to the diameter of the cable to be positioned in between the spades. The cutting process induces the suspension of the soil between the spades.
- The sediment transport area, downstream of the ROV: the soil is mixed with the water and entirely disturbed. Sedimentation occurs due to the action of gravity.

Numerous laboratory experiments on subsea jet trenching methods exist, to predict the depth of the trench created, the jet pressure needed, etc. by mathematical formulas. Several examples can be cited, such as one of the first studies on the subject done by Rouse (1940) [9], where the impact of the composition of the sediment and the jetting strength on the shape of the trench was studied. Yeh et al. (2008) [10] have made a study on the impact of moving circular vertical jets on the sea floor. The study is made in a large-scale laboratory experiment to predict the cavity geometry with mathematical formulas. Their development is based on empirical formulas developed by Chiaia et al. (1997) [11]. Dong et al. (2020) [12] have analysed digging in cohesive soils with vertical jets in a laboratory experiment, to see the dependence of the dredging on the sediment composition, on the duration of the jets, etc. B. Westrich and H. Kobus (1973) [13] have studied the erosion of a sand bed by continuous and pulsating jets. In the study, they show that the rate of erosion is dependant on the momentum flux of the jet and the distance between the sand bed and the nozzle. Other similar studies on trenching in cohesive soils are numerous, such as the experiments of Zhang et al. (2017) [14] to predict the trench geometry depending on the nozzle diameter. Another study has also been made to see the impact of jetting on a non-uniform sand bed, by W. Mih and J. Kabir (1983) [15].

Numerical methods have also been introduced to analyse jet trenching and sediment transportation, since it is easier to retrieve specific information with computational fluid dynamics, such as the static pressure on the jetting system. Yan et al. (2020) [16] have studied a sediment-scour model using OpenFOAM and the moving mesh technique. Franz et al. (2017) [17] implemented a model to predict the sediment transport and the evolution of the bed depending on the sediment type. The implementation was done using MOHID, a modelling system solving the advection and transportation of suspended sediment. Wang and Song (2019) [18] have studied a continuous jet excavation process with computational fluid dynamics, using the Herschel-Bulkley model for the cohesive soil. Wang et al. (2021) [19] have looked at moving vertical jets eroding cohesive soils, implementing a computational fluid dynamics model to look at the trenches created, depending on the shear strength, the velocity of the jets and the hydrodynamic pressure of the jets. The cohesive soil was implemented with the Bingham Plastic Model, to represent non-Newtonian fluids. OpenFOAM was the tool used to solve the numerical model.

A.T.H. Perng and H. Capart (2008) [1] have investigated plane jets directed to a non cohesive soil, a situation close to the one introduced in this thesis. They have simplified the problem described by figure 1.2 by studying plane jets moving at constant velocity. Their study is based on laboratory experiments, where the velocity of the vehicle and the jetting strength are the main analysed parameters that impact the trench depth and shape. In the article, the results obtained in the laboratory are compared to a mathematical model called the sub-layered shallow flow theory. The results of those experiments are used in this thesis to validate the developed numerical model.

The jetting system and the induced sedimentation of the soil are implemented using the open-source software Migflow [20]. That tool solves immersed granular flows, thus solid discrete bodies, the grains, submerged in a fluid. This has numerous applications in engineering, chemical industry and other fields. Immersed granular flows can be, for example, concrete or a mix of a cream with a powder. Here it would represent the particles of the sediment immersed in seawater. The finite element method is used to solve the fluid part of the problem, at a greater scale than the grains. The grains are solved using the discrete element method. To transit between the two states, the Navier-Stokes equations are averaged using the fluid volume fraction.

In that way, the mixture is continuous and thus the domain can be represented by one continuous mesh. In this thesis, the grains are not used to model the problem since the sediment is approximated by a Newtonian fluid, thus the averaged Navier-Stokes equations are averaged with a volume fraction of 1, which does not change the equations from their non-averaged form. Some modifications are brought to the code to fit the requirements of the analysed problem. The meshes are generated using the tool Gmsh [21].

This thesis is a preliminary study whose purpose is to see if the results of the laboratory experiments of A.T.H. Perng and H. Capart can be obtained with the software Migflow. With that goal in mind, this thesis is divided into different parts. First, the equations solved by and added to the software are given and explained. Solving such a situation brings different problems that have to be formulated in equations, such as the sedimentation of the soil. Then, the numerical model based on the small-scale experiment of Perng and Capart is explained in detail, giving the geometry of the laboratory experiment, the simplified 2D geometry used here and detailing the mesh used. In that section is also given a stability analysis, an analysis of the parameters influencing the simulations and a comparison to the laboratory results. Finally a conclusion will be drawn, comparing the results obtained using Migflow and the ones obtained by Perng and Capart via laboratory experiments.

Chapter 2

The equations

To obtain numerical simulations of the dredging system and of the formation of a trench to bury a cable, the governing equations of the problem must be identified. In the simulations, the water and the sediment are both assumed to be incompressible fluids, but with different properties.

In the software Migflow, the equations computed give the evolution of the fluid and of the grains. The physical fields are computed using the Navier-Stokes equations averaged using the porosity ϕ, which represents the volume fraction of fluid compared to the volume fraction of grains, inside a control volume [20]. Writing the mean velocity of the fluid phase $\mathbf{u} = \phi\mathbf{v}$, where $\mathbf{v}$ is the advection velocity, the conservation laws for the fluid phase are given by equation 2.1 and equation 2.2 [20].

$$\rho\left(\frac{\partial \mathbf{u}}{\partial t} + \nabla \cdot \frac{\mathbf{u}\mathbf{u}}{\phi}\right) = \nabla \cdot [2\mu\phi\mathbf{d}(\mathbf{u}) - p\mathbf{I}] + f + \phi\rho\mathbf{g} \tag{2.1}$$

$$\frac{\partial \phi}{\partial t} + \nabla \cdot \mathbf{u} = 0 \tag{2.2}$$

Where ρ is the density of the fluid and is assumed constant, μ is the dynamic viscosity of the fluid, p is the pressure, $\mathbf{I}$ is the identity tensor, f is the force density coming from the fluid-grains interaction, $\mathbf{g}$ is the vector representing the gravity and $\mathbf{d}(\mathbf{u})$ is the rate of deformation tensor:

$$\mathbf{d}(\mathbf{u}) \triangleq \frac{1}{2}\left[\nabla\frac{\mathbf{u}}{\phi} + \left(\nabla\frac{\mathbf{u}}{\phi}\right)^T\right]$$

Since the problem contains only incompressible fluids and the grains are not considered in this study, the conservation laws can be simplified, with $\phi = 1$. It gives the well-known Navier-Stokes equations inside a control volume, equation 2.3 and the incompressibility hypothesis, equation 2.4.

$$\rho\left(\frac{\partial \mathbf{v}}{\partial t} + \nabla \cdot [\mathbf{v}\mathbf{v}]\right) = \nabla \cdot [2\mu\mathbf{d}(\mathbf{v}) - p\mathbf{I}] + \rho\mathbf{g} \tag{2.3}$$

$$\nabla \cdot \mathbf{v} = 0 \tag{2.4}$$

Where $\mathbf{d}(\mathbf{v})$ is the rate of deformation tensor and is equivalent to $\mathbf{d}(\mathbf{u})$:

$$\mathbf{d}(\mathbf{v}) \triangleq \frac{1}{2}\left[\nabla\mathbf{v} + (\nabla\mathbf{v})^T\right]$$

Those equations are already implemented in the software Migflow and a first test is made on a simple mesh, figure 2.1a. The mesh is a rectangle, of height 15 [m] and of width 20 [m]. The sword is 3 [m] long. The

size of the elements is 15 [cm] at the sword and 45 [cm] far from the sword. The ROV moves at horizontal velocity of 5 [$\mathrm{m\,s^{-1}}$] and the vertical velocity at the jet is 30 [$\mathrm{m\,s^{-1}}$]. The vertical velocity at the boundaries is null. The magnitude of the horizontal velocity at the boundaries is the same as the velocity of the ROV. The fluid is water, of density 10^3 [$\mathrm{kg\,m^{-3}}$] and viscosity 10^{-6} [$\mathrm{m^2\,s^{-1}}$]. The exact values are not important here, since the test is made only to see the result of the two main equations applied to the problem, with only one fluid, thus with no sediment. Those two equations, 2.3 and 2.4, have not been modified for the purpose of this thesis. The result is given figure 2.1b. The result is conform to reality. The jet forms vortices and those are translated due to the horizontal velocity of the vehicle.

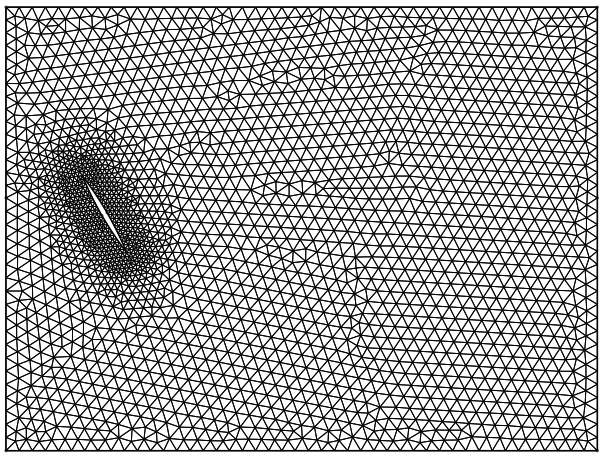

(a) Mesh

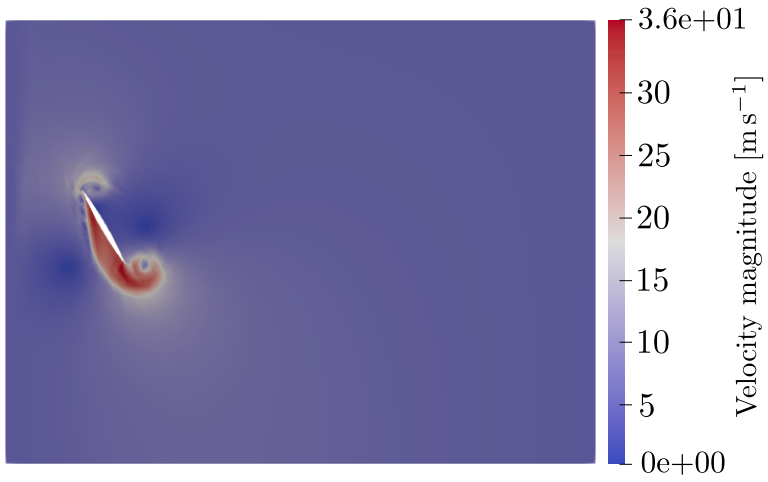

(b) Result of the simulation: velocity magnitude

Figure 2.1: First test: problem with one fluid

Now that the result is tested with one fluid, the equations must be completed to take into account the differences brought by considering two fluids in the problem instead of only one. Therefore, those equations are combined with a concentration equation, explained in section 2.1. Because the fluids have different densities, a sedimentation velocity is included in the concentration equation, as explained in section 2.2.

2.1 Concentration equation

Since the problem requires the sediment and the water to mix, the concentration of both sediment and water must be determined. This is done with the concentration equation, given by equation 2.5. That equation gives the evolution of a, the concentration of one of the two fluids, with time. The concentration of the other fluid can be obtained by the simple computation $1 - a$.

$$\frac{\partial a}{\partial t} = \underbrace{-\nabla \cdot (\mathbf{v}a)}_{\text{Advection}} \underbrace{-\kappa \nabla^2 a}_{\text{Mass diffusion}} \tag{2.5}$$

Where $\mathbf{v}$ is the advection velocity and κ is the mass diffusivity coefficient. The equation expresses two phenomenons: the advection and the mass diffusion of the concentration.

This advection part of equation 2.5 can be further simplified to obtain equation 2.6.

$$\begin{aligned} \text{Advection} &= -\mathbf{v} \cdot \nabla a - a \nabla \cdot \mathbf{v} \\ &= -\mathbf{v} \cdot \nabla a \end{aligned} \tag{2.6}$$

The difference between the advection part of equation 2.5 and equation 2.6 is the following: the first formulation is what can be called the conservative form of the advection equation. Indeed, for the solving of the Navier-Stokes equations to be stable, the divergence of the velocity cannot be exactly null and thus the incompressibility hypothesis, equation 2.4, cannot be respected. The second form can be called the consistent form of the advection equation. It assumes that the divergence of the velocity is indeed null, rejecting the hypothesis of conservation. Considering the fact that, in this problem, the domain is open, it can be concluded that conservation is not a requirement. Hence, the consistency hypothesis is the one applied in the simulations.

The mass diffusion part of the equation is added to create diffusion between the two fluids. It is added here to impact the boundary between the two fluids. Because the simulations are done on triangular meshes, that boundary usually follows the shape of the elements, making the result appear unrealistic. Adding the mass diffusion term in the concentration equation adds thus a blurring effect at the boundary between sediment and water. The impact of this term is discussed in the following chapter.

2.2 Sedimentation velocity

Having a mixture of two fluids of different densities implies the introduction of a sedimentation velocity. When mixing two fluids where one has a higher density than the other one, the heavier fluid should slowly settle on the lower boundary, the floor, due to the action of gravity on each heavier fluid particle. In this thesis, the two fluids are water, the lighter one, and sand, the heavier one.

The velocity of settlement is what will be called here the sedimentation velocity. In this section, a formula for that velocity will be given and validated. From here, a will represent the concentration of water, the lighter fluid, and $\mathbf{w}$ the sedimentation velocity. For the expression to be consistent with reality, it must verify two conditions:

1. The magnitude of the sedimentation velocity decreases if the concentration of the sand increases:
   $|\mathbf{w}| \searrow$ when $(1 - a) \nearrow$ or
   $|\mathbf{w}| \nearrow$ when $a \nearrow$
2. If no sand is present in the water, the sedimentation velocity must be null:
   $\mathbf{w}(a = 1) = 0$

The sedimentation velocity, $\mathbf{w} = 0\ \mathbf{e}_x + w\ \mathbf{e}_y + 0\ \mathbf{e}_z$, can be expressed by equation 2.7.

$$w = = C\ g\frac{\rho_{\text{water}} - \bar{\rho}}{\rho_{\text{water}}} \qquad \text{where } \bar{\rho} = \rho_{\text{water}} a + \rho_{\text{sand}}(1-a) \tag{2.7}$$

Where $C > 0$ is a constant, $g = -9.81\ [\mathrm{m\,s^{-2}}]$ represents the gravity in the vertical direction, $\mathbf{e}_y$, ρ_{water} is the density of water and ρ_{sand} is the density of sand. Those densities are assumed constant, making the sedimentation velocity a linear function of the concentration of water only.

The first step is to verify those two conditions explained above. The sedimentation speed, the norm of the sedimentation velocity, should decrease if the concentration of the heavier fluid increases, as given by the first condition. This is proven by equation 2.8, with $\rho_{\text{sand}} > \rho_{\text{water}}$.

$$\begin{aligned} \frac{\mathrm{d}|\mathbf{w}|}{\mathrm{d}a} &= C\ |g| \left[-\frac{\mathrm{d}\bar{\rho}}{\mathrm{d}a} \frac{1}{\rho_{\text{water}}} \right] \\ &= -C\ |g| \frac{\rho_{\text{water}} - \rho_{\text{sand}}}{\rho_{\text{water}}} > 0 \end{aligned} \tag{2.8}$$

Equation 2.8 is illustrated figure 2.2 by the slope of the curve of the sedimentation speed.

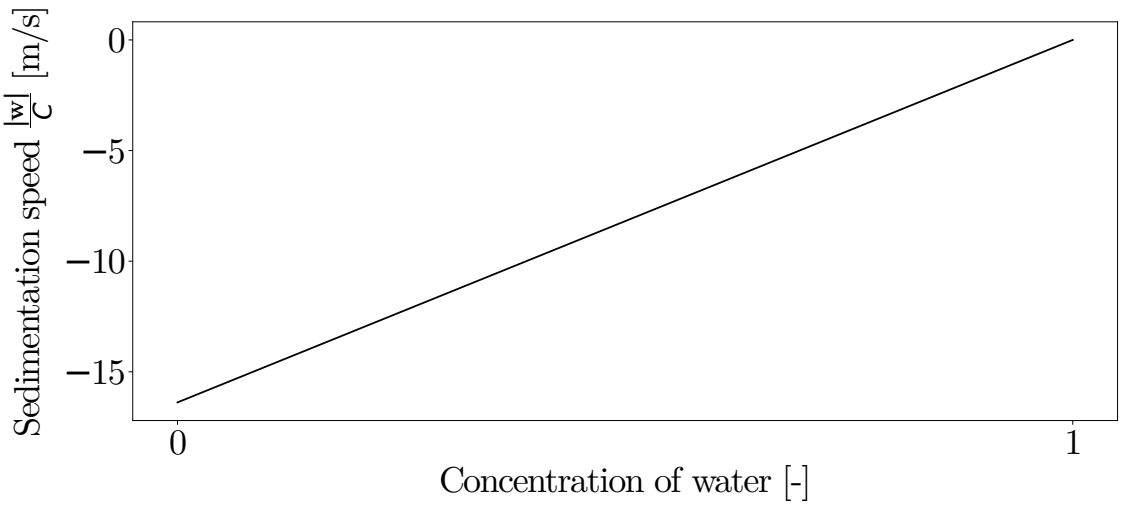

Figure 2.2: Evolution of the sedimentation speed with the concentration of water

The second condition is verified by replacing a by 1 in equation 2.7. In that case, the sedimentation velocity is indeed null.

Now that the expression of the sedimentation velocity is determined and the conditions to validate the expression are verified, the validation through simulations can start.

First, this expression for the sedimentation velocity is applied and validated on a simple 1D advection problem, using a discretization scheme to discretize the equation in time and in space. Then, the sedimentation velocity is inserted in the concentration equation of the main problem, in the software Migflow. Next, a discussion is made about the resolution of the flux term between two elements when solving the concentration equation. In that discussion are presented the related simulations on a simple 2D problem, to see the impact of that flux term and validate the reasoning.

2.2.1 Validation of the sedimentation velocity: equation in 1D

The sedimentation is tested with equation 2.9, a 1D advection equation.

$$\frac{\mathrm{d}a}{\mathrm{d}t} = -\frac{\mathrm{d}\left[w(a)a\right]}{\mathrm{d}z} \tag{2.9}$$

Where z is the vertical component, a is the value of the concentration of water and w is the sedimentation velocity as given by equation 2.7. As said before, that velocity is dependent on the concentration only.

To solve numerically that equation on a simple 1D problem and find the value of a at each node and each time step, the expression must be discretized. Once discretized, boundary conditions must be applied to obtain a coherent result.

Discretisation of the advection equation

The discretisation of equation 2.9 is done using the Richtmyer two-step Lax–Wendroff method [22], as given by equation 2.10, where index i represents the spatial index and j the temporal index. That scheme is chosen because it is used to solve non-linear transport equations, thus transport equations where the coefficient, here w, is dependent on the advected variable, here a.

$$\begin{aligned}
a_{i-\frac{1}{2}}^{j-\frac{1}{2}} &= \frac{1}{2}\left(a_i^{j-1} + a_{i-1}^{j-1}\right) - \frac{\Delta t}{2\Delta z}\left(w_i^{j-1}a_i^{j-1} - w_{i-1}^{j-1}a_{i-1}^{j-1}\right) \\
a_{i+\frac{1}{2}}^{j-\frac{1}{2}} &= \frac{1}{2}\left(a_i^{j-1} + a_{i+1}^{j-1}\right) - \frac{\Delta t}{2\Delta z}\left(w_{i+1}^{j-1}a_{i+1}^{j-1} - w_i^{j-1}a_i^{j-1}\right) \\
a_i^j &= a_i^{j-1} - \frac{\Delta t}{\Delta z}\left(w_{i+\frac{1}{2}}^{j-\frac{1}{2}}a_{i+\frac{1}{2}}^{j-\frac{1}{2}} - w_{i-\frac{1}{2}}^{j-\frac{1}{2}}a_{i-\frac{1}{2}}^{j-\frac{1}{2}}\right)
\end{aligned} \tag{2.10}$$

Where Δz is the spatial step and Δt is the time step. This scheme is of second-order accurate and is conservative.

Boundary conditions

The 1D domain is considered closed, so both upper and lower boundaries can be thought as walls. This implies that at both upper and lower boundaries, the flux going in and out of the volume must be zero. The heavier fluid will therefore accumulate at the lower boundary and the lighter fluid will get pure at the upper boundary.

Assuming i increasing while going up ($i = 0$ is thus the lower boundary), the boundary conditions can be expressed with equation 2.11 and equation 2.12.

$$\text{Upper boundary: } a_{i+\frac{1}{2}}^{j-\frac{1}{2}} = 0 \tag{2.11}$$

$$\text{Lower boundary: } a_{i-\frac{1}{2}}^{j-\frac{1}{2}} = 0 \tag{2.12}$$

The result is given figure 2.3. At time $t = 0$, the mixture is made of 50% of sand and 50% of water, homogeneously mixed together. Gravity acts on the sand particles, since they are the heaviest when compared to the water particles, and they settle on the floor of the domain, at $z = 0$, increasing the thickness of pure water layer at the top, until the entirety of the sand has settled. As expected since no diffusion is implemented, the graph is symmetric around the horizontal line $\frac{z}{z_0} = 0.5$. It shows a correct sedimentation behaviour and the expression of the sedimentation velocity can be implemented in the real problem, using Migflow.

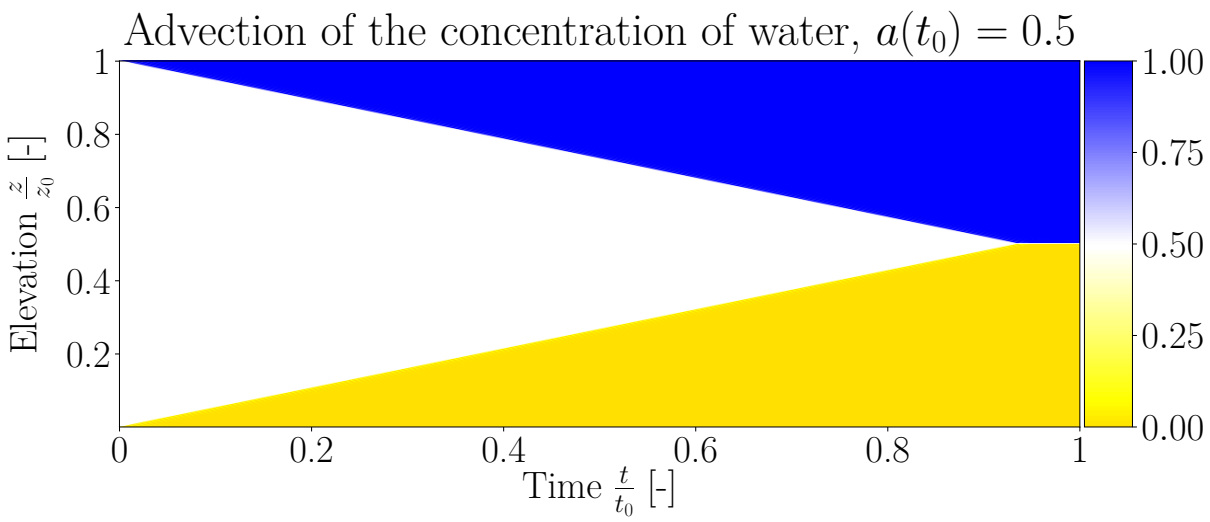

Figure 2.3: Testing of the sedimentation velocity on a simple 1D problem

2.2.2 Insertion of the sedimentation velocity in Migflow

This velocity $\mathbf{w}$ is added to the advection part of the conservative formulation of the concentration equation, equation 2.5, and it becomes equation 2.13.

$$\frac{\partial a}{\partial t} = -\nabla \cdot [(\mathbf{v} + \mathbf{w})a] - \kappa \nabla^2 a \tag{2.13}$$

That formulation stays conservative. The same simplification as before can be applied to equation 2.13, obtaining equation 2.14, the consistent formulation of the concentration equation with sedimentation.

$$\begin{aligned} \frac{\partial a}{\partial t} &= -(\mathbf{v} + \mathbf{w}) \cdot \nabla a - a \nabla \cdot (\mathbf{v} + \mathbf{w}) - \kappa \nabla^2 a \\ &= -(\mathbf{v} + \mathbf{w}) \cdot \nabla a - a \nabla \cdot \mathbf{w} - \kappa \nabla^2 a \end{aligned} \tag{2.14}$$

Equations 2.13 and 2.14 are advection-diffusion equations.

2.2.3 Flux term between two elements

Now that the sedimentation velocity has been tested on a 1D problem and introduced in the equations next to the Navier-Stokes equations and to the incompressibility hypothesis, it can be implemented in the software Migflow. For that, in the concentration equation, the flux term between each element must also be computed. This, as will be explained in this section, led to difficulties regarding the advection part of the equation.

To do so, the advection part of equation 2.13 is first decomposed into two different pieces and is rewritten as equation 2.15. Indeed, a distinction is possible and needed for the rest of the development, since $\mathbf{v}$ is independent of a but $\mathbf{w}$ is a function of only a.

$$\text{Advection} = \underbrace{-\nabla \cdot [\mathbf{v}a]}_{(1)} \underbrace{-\nabla \cdot [\mathbf{w}a]}_{(2)} \tag{2.15}$$

In general, in an advection equation with constant coefficient, as in equation 2.16, the sign of the coefficient, B, determines on which side of the boundary between elements the information for a is taken, when discretizing.

$$\frac{\partial a}{\partial t} = -B \frac{\partial a}{\partial x} \tag{2.16}$$

Indeed, the equation being an advection equation, the information to compute the value of a at the next time step must be taken from where it comes, upwind. If the coefficient is positive, $B > 0$, the advection equation is computed using backward differences. If the coefficient is negative, $B < 0$, the advection equation is computed using forward differences. Both one-sided finite differences are illustrated figure 2.4.

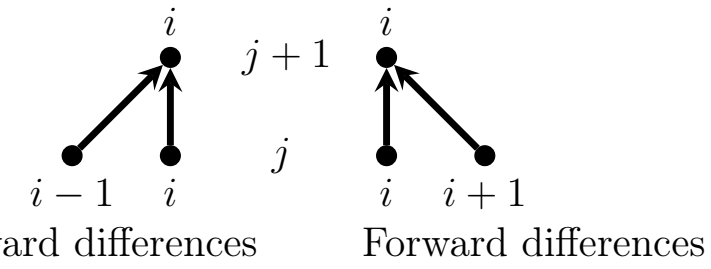

Figure 2.4: Illustration of one-sided finite differences on a mesh, where i is the spacial index in 1D, j is the temporal index and the dots represent the nodes on the mesh

However, in this situation, the coefficients in the advection equation are not constant. Part (1) of equation 2.15 is a simple linear advection equation, where $\mathbf{v}$ is a function of $\mathbf{x}, t$, but not a. Therefore, the sign of $\mathbf{v}$ dictates if the information for a at the boundaries is taken using backward **or** forward differences, as in an advection equation with constant coefficient.

The second part of equation 2.15 is the trickiest part of the equation. To understand the development and see the impact of the reasoning, tests have been executed. The mesh for the tests is first described, followed by the reflection on that second part of the equation.

Description of the mesh for the tests

To test the implementation of the sedimentation velocity in the code of Migflow, several simulations have been made on a simple 2D problem, without the mass diffusion part of the equation. The mesh, figure 2.5, is a square of size 1 [m]. The size of each element is 2 [cm] and is constant across the mesh. It is small so the boundary at the end of the simulation is as straight as possible, since the solution follows the shape of the elements. The behaviour of the sedimentation would be similar if done on a mesh with bigger sizes for the elements.

Each simulation starts with 50% of water and 50% of sand homogeneously mixed together. This means that it starts with with a concentration $a = 0.5$ everywhere and null horizontal and vertical velocities. The square is considered to be a closed box, so there is no flux through the boundaries of the domain and the velocity vectors at the boundaries are null. Because of sedimentation, the sand should settle on the lower boundary of the square, obtaining the same result as the one in 1D but this time in 2D. Hence, at the lower boundary, the level of pure sand should increase upwards while, at the upper boundary, the level of pure water should increase downwards. The data for each simulation is given table 2.1.

ρ_{water} $[\text{kg m}^{-3}]$	ρ_{sand} $[\text{kg m}^{-3}]$	ν_{water} $[\text{m}^2\,\text{s}^{-1}]$	ν_{sand} $[\text{m}^2\,\text{s}^{-1}]$	C $[-]$
1000	2670	10^{-6}	10^{-4}	1

Table 2.1: Data for the simulations relative to the computation of the flux term between two elements

The sand is thus heavier than the water and more viscous, to reflect reality. The density of the sand is the one used by Perng and Capart in their experiments [1]. The coefficient of sedimentation affects only the time taken for the entirety of the sand to settle and its value is thus not the most important in the tests.

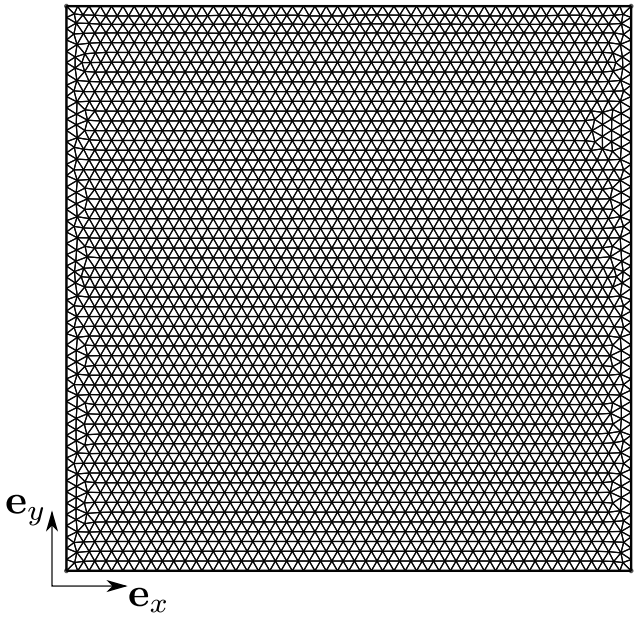

Figure 2.5: Simple squared mesh

Reflection process and simulations

A first thought was to compute the part (2) using forward or backward differences, depending on the sign of $\mathbf{w}$. Since $\forall a, w \geq 0$, it means that it should be computed using only backward differences. This method is similar to the one used to compute part (1) and it gives the result presented figure 2.6. In the simulation, the particles of sand fall due to gravity, raising the level of pure sand at the lower boundary. But the problem is that, while the particles of sand fall, the water is not cleared of the sand and the thickness of pure water at the upper boundary stays small and constant. This creates a problem of conservation: at the end of the simulation, the square is filled with only pure sand and the water has disappeared. This means that sand has been created and water has been lost, even though the domain is surrounded by walls. This wrong result makes sense: for the water to be cleared from the sand and thus for the thickness of the water layer to increase, a forward difference would be needed, since the sedimentation velocity is positive in the $\mathbf{e}_y$ direction. This shows that using only backward differences for the sedimentation velocity leads to wrong results.

Another test has thus been carried out, where part (2) was computed using the opposite method of part (1). Because the sedimentation velocity is positive, whatever the value of the concentration of water, this means that the test is done using forward differences to compute part (2). The simulation is unstable and the result is presented figure 2.7. At time $t = 0$ [s], the initial condition is the same as in figure 2.6.

Both simulations are wrong but they both show good behaviour in some aspects. On the first one, the level of sand rises correctly. On the second one, even if it is unstable, the water gets cleared of the sand. The following step would thus be to combine those two results to obtain a final correct simulation.

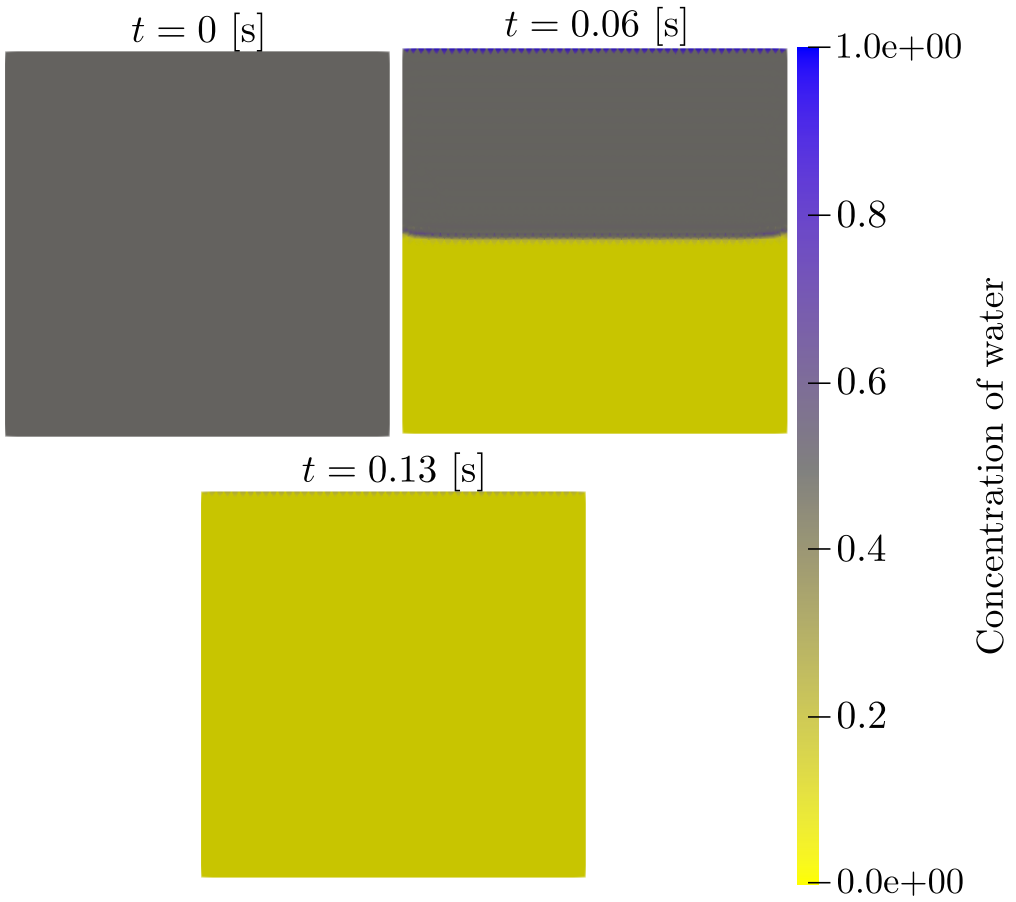

Figure 2.6: Evolution of the concentration of water: backward differences, since $\mathbf{w} \geq 0$

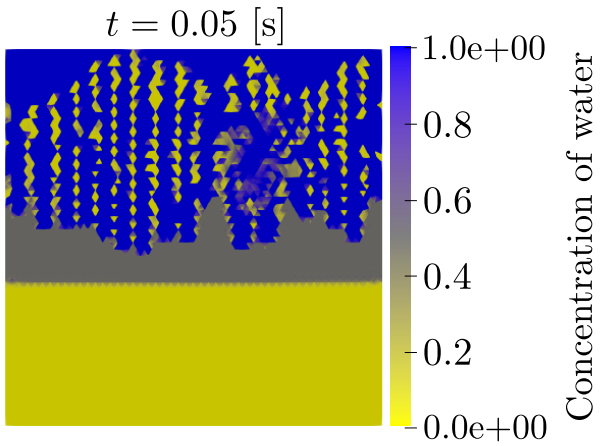

Figure 2.7: Evolution of the concentration of water: forward differences

Before trying another simulation without a real thought process behind, it is useful to look at the equations and develop them to find a justification and a solution to what is observed. After finding that mathematical justification, it is tested on the same simple 2D problem.

Part (2) has to be developed further since $\mathbf{w}$ is a function of a. First, equation 2.7 can be rewritten to obtain equation 2.17, a simple linear function of the concentration.

$$\begin{aligned} w &= C\ g\frac{\rho_{\text{water}} - \rho_{\text{sand}}}{\rho_{\text{water}}}(1-a) \\ &= A(1-a) \end{aligned} \tag{2.17}$$

Where $A > 0$ is a constant. Introducing that result into part (2) of equation 2.15 gives equation 2.18, after some development.

$$\begin{aligned} (2) &= -A\frac{\partial[(1-a)a]}{\partial y} \\ &= -A\frac{\partial[a-a^2]}{\partial y} \\ &= 2A\left(-\frac{1}{2}\frac{\partial a}{\partial y} + a\frac{\partial a}{\partial y}\right) \end{aligned} \tag{2.18}$$

This result is a combination of a linear advection equation with constant coefficient, where the coefficient is negative, and of a Burgers' equation. a is a function of x, y, t but here it will be written as a function of y, t to simplify the notations, as there is not partial derivative with respect to x in the equations analysed.

The solution to the linear advection equation with constant coefficient, equation 2.16, can be found using the characteristics method [23]. First, a is conserved along each characteristic, whose direction is $dy = Bdt$. Considering an open (unbounded) system, the Cauchy problem is defined by the following initial condition: $y(s) = s$ and $t(s) = 0$. The function f is defined as $f(s) = a(y(s), t(s)) = a(s, 0)$ and is given. The direction of the characteristics is then integrated to give the result given by equation 2.19, since B is constant.

$$\int_s^y dy' = B\int_0^t dt' \Rightarrow y - s = Bt \tag{2.19}$$

The solution is $a(y, t) = f(y - Bt)$ where $B = -\frac{1}{2}$ in this case and is **negative**. The flux term between two elements is thus computed using forward differences here.

The same reasoning can be used for the Burgers' equation, where $dy = a(y, t)dt$ and $f(s) = a(s, 0) = a(y, t) \Rightarrow dy = f(s)dt$. The integration of the direction of the characteristics is given by equation 2.20.

$$\int_s^y dy' = f(s)\int_0^t dt' \Rightarrow y - s = f(s)t \tag{2.20}$$

The solution is $a(y, t) = f(y - a(y, t)t)$. Since $0 \leq a(y, t) \leq 1$, the coefficient is **positive** $\forall y, t$. The flux term between two elements is thus computed using backward differences here.

To sum-up that mathematical reasoning, since the second part of the equation contains two kind of advection equations with coefficients of opposite signs, the information to compute the concentration must be taken using backward **and** forward differences.

Using that reasoning in the code, the result is presented figure 2.8. At time $t = 0$ [s], the initial condition is the same as in figure 2.6. In the simulation, the level of pure sand rises while the water gets cleared of the sand, as it should. As expected, since no diffusion is implemented and as in 1D, the result is symmetric around the horizontal line $\frac{y}{y_0} = 0.5$. The stationary state of the simulation is the square filled with half of pure sand and half of pure water, as expected. The boundary between sand and water is as straight as possible, following the edges of the elements.

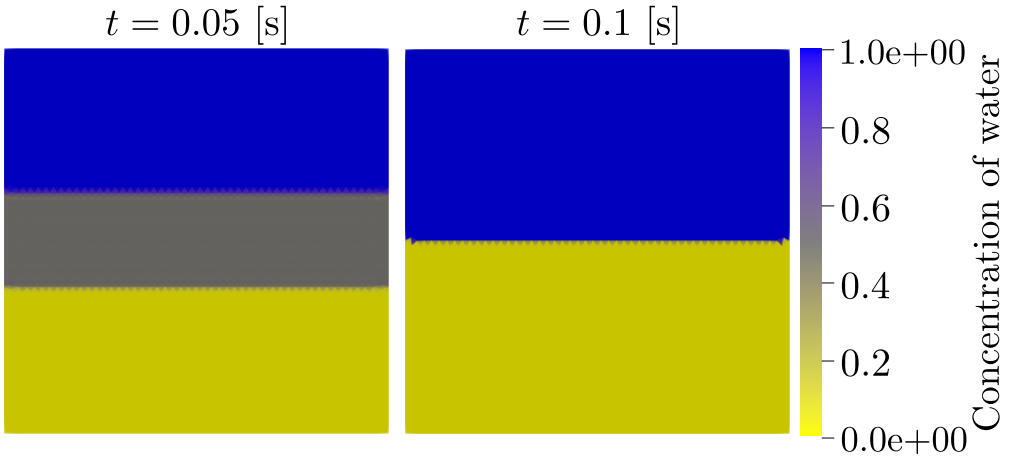

Figure 2.8: Evolution of the concentration of water: forward and backward differences

In conclusion, the reasoning through equations shows that both forward and backward differences are needed to compute the second part of the advection equation. The simulations on a simple 2D problem confirm that reasoning. That problem of forward or backward differences for the computation of the flux term between two elements did not appear in the 1D problem because the scheme chosen to solve the 1D advection equation is one that solves non-linear equations. The equation 2.10 is indeed a combination of forward and backward differences, using an intermediate time step. Now that all equations to solve the problem are determined and tested, the reproduction of the experiment setup and the results are examined.

Chapter 3

Numerical model of the Perng and Capart's experiment

A.T.H. Perng and H. Capart have experimented a jetting system in a small-scale laboratory. The goal of their experiment was to determine the water and the sediment motion caused by the travelling plane jets along the sea bed depending on the velocity of the vehicle and on the jetting strength. Once the experiments done, the results were compared to a theory developed in the article, called the sub-layered shallow flow theory. The setup is detailed in their article [1] and is reproduced numerically here.

First, the geometry and dimensions of the domain in the numerical problem compared to the ones in the laboratory will be described, as well as the mesh used in the numerical simulations. Then, a stability analysis will be carried out to determine the order of the time step relative to the size of the mesh and the critical velocity of the problem. Finally, a study will be done to analyse the influence of different parameters to the numerical simulations and see if the results using Migflow and the different equations developed in this study are close to the results of the small-scale laboratory experiment.

3.1 Definition of the domain and mesh

The laboratory experiment takes place in a 3D rectangular tank, with a height of 50 [cm], with a length of 180 [cm] and with a width of $B = 12.6$ [cm]. The bottom 18 [cm] in the tank are pure sand of density $\rho = 2670$ [kg m^{-3}], and on top of that sand is 29 [cm] of water, of density $\rho = 1000$ [kg m^{-3}] and kinematic viscosity $\nu_{\text{water}} = 10^{-6}$ [m^2 s^{-1}]. The rest of the tank is just air. The jetting system is made of three cylinders placed side by side, each made of 19 nozzles with a diameter of 0.5 [mm], separated by 2 [mm] and at an angle α of 30° from the vertical. Instead of being buried in the sand like on figure 1.2, the jets are at a vertical distance Z from the sand. Another difference to the case presented figure 1.2 is the angle of the jets, here at angle $\alpha = 30°$ from the vertical and not completely vertical. The jetting system travels at constant speed U from the right of the tank to the left. A system at the top of the tank is used to keep the level of the water constant, when the jets are on. Drawings of the laboratory setup are given figure 3.1.

The differences between the laboratory experiment and the geometry used in this thesis are the following: the setup here is reduced to a 2D problem, modifying the three cylinders and 3×19 nozzles to one circle with one nozzle. The different dimensions respect the ones in the laboratory and are given figure 3.2. The radius of the circle is set to 2 [cm]. The sand, in the simulations, is approximated by a Newtonian fluid and its viscosity is chosen so its behaviour is close to the behaviour of real sand.

The laboratory experiment used velocities in the range from 0 to 10 [cm s^{-1}] for the horizontal velocity of the ROV, U. These values are used in the simulations. In the laboratory, the vehicle travelled at speed U

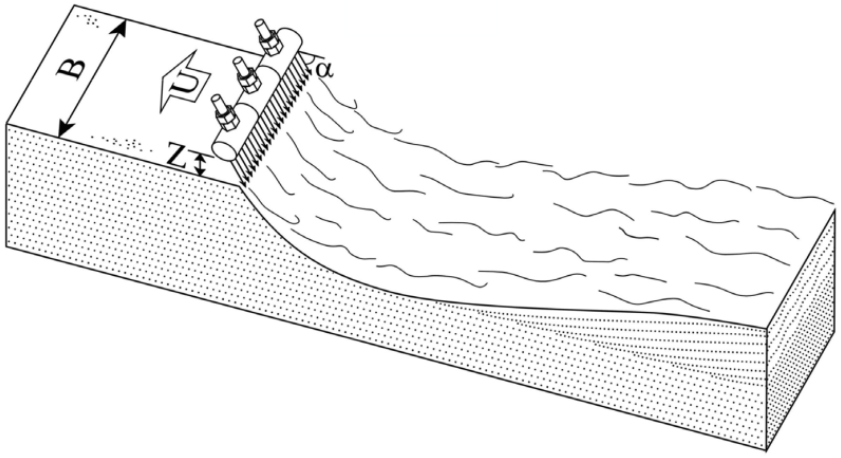

(a) 3D drawing

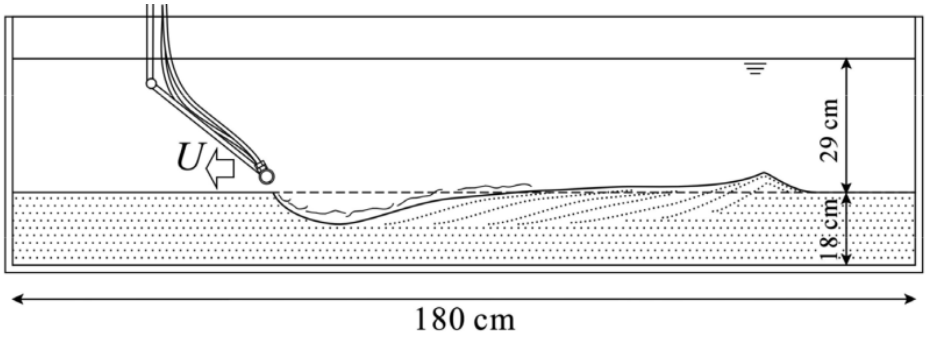

(b) 2D drawing

Figure 3.1: Setup of the laboratory experiment, image taken in [1]

from the right to the left of the tank. In the simulations, the vehicle, represented by the circle, is fixed and the domain moves from left to right at the same speed, renamed U_0. This avoids regenerating the mesh at every time step to move the circle at constant velocity U_0. This is the reason why the whole domain is not needed for the simulations. Those are instead made on the zoomed part of the domain, figure 3.2.

Since the simulations are in 2D and the nozzles are reduced to one 2D jet, the velocity V at the jet must be adapted to have the same flux in the laboratory experiments and in the simulations. In the laboratory, the flux varied between three values: $Q = 90,\ 107$ and $122\ [\mathrm{mL\,s^{-1}}]$. The velocity is thus computed using equation 3.1, where B is the width of the tank in the laboratory experiment and D_{jets} is the diameter of the jets.

$$V = \frac{Q\ [\mathrm{m^3\,s^{-1}}]}{B[\mathrm{m}]\ D_{jets}[\mathrm{m}]} \tag{3.1}$$

In the simulations, boundary conditions are needed at each boundary of the domain and are described figure 3.2. The difference of pressure at the upper boundary in the simulations is null and the boundary is open, meaning that a flux, of water for example, can go through the boundary. At the left, right and bottom boundaries, the horizontal velocity is the one of the vehicle and the vertical velocity is null. The left and right boundaries are also open, since the smaller domain is moving inside the bigger one representing the tank. The lower boundary is a wall, meaning that there is no flux through that boundary.

The mesh, generated using Gmsh, is presented figure 3.3.

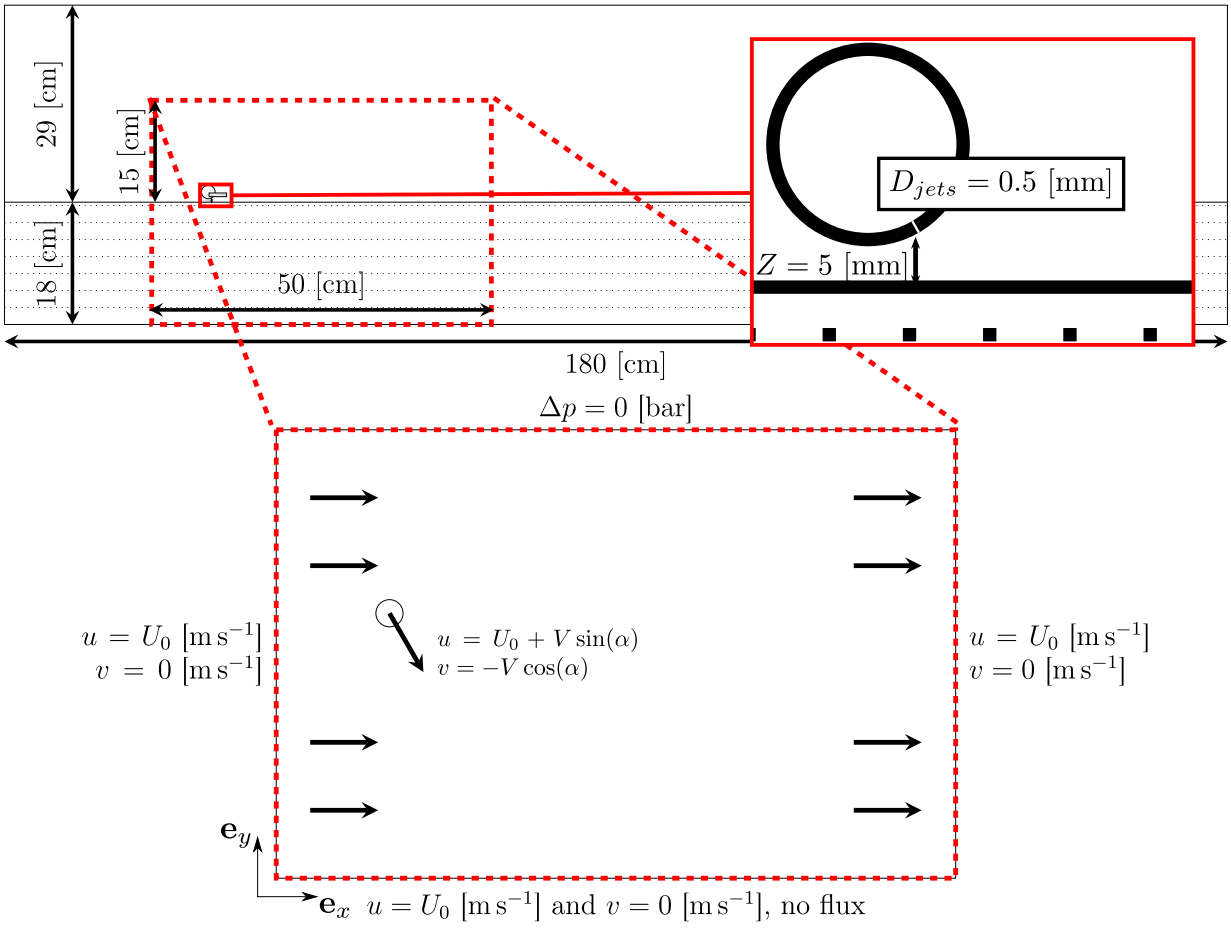

Figure 3.2: Dimensions and boundary conditions reproducing the experiment setup and used for the simulations

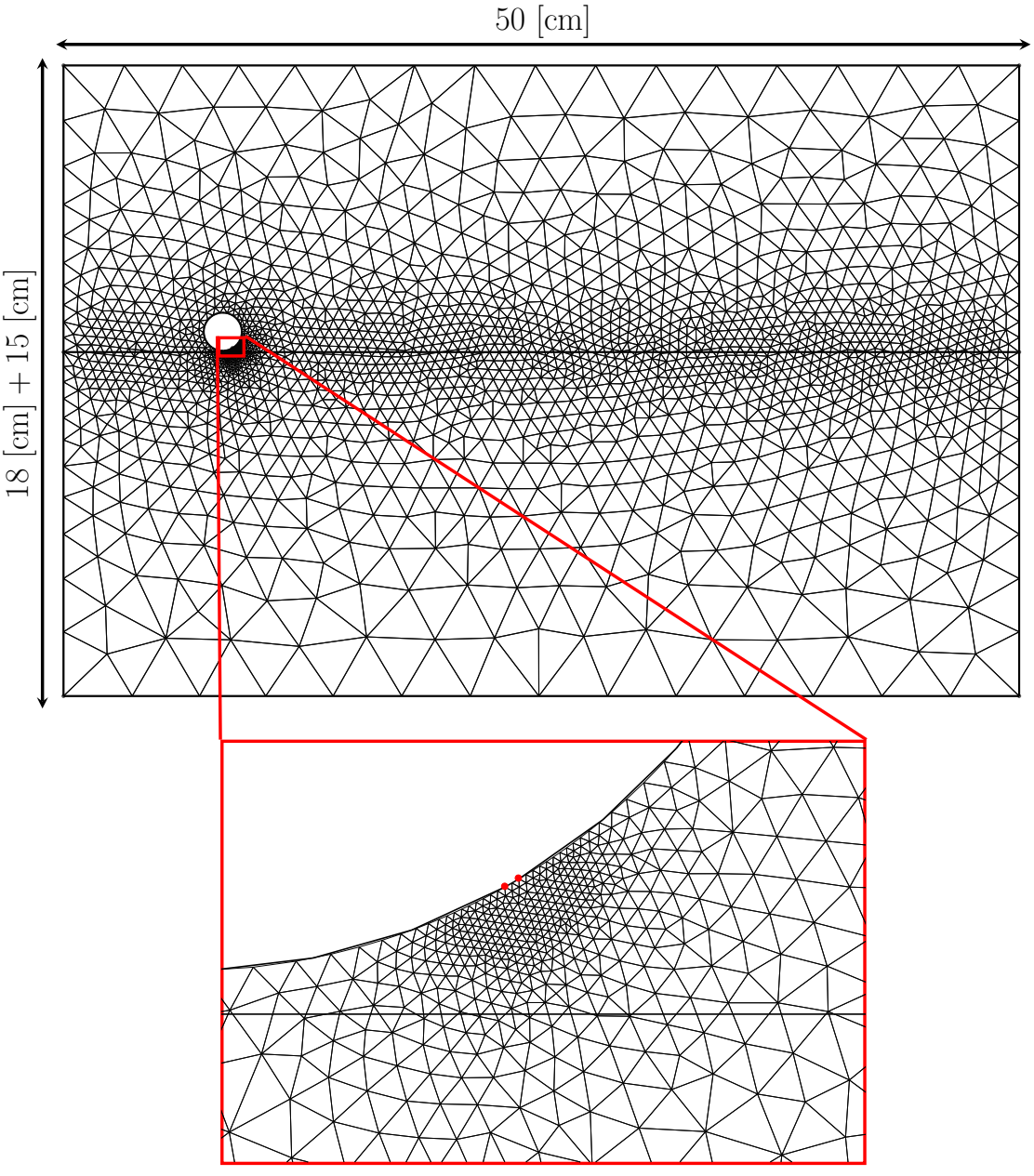

Figure 3.3: Mesh used in the simulations

On the mesh, the horizontal line in the middle is a fictive line that delimits the sand and the water at rest at time $t = 0$ [s]. The size of the elements is determined from two conditions:

1. Close to that fictive line, the elements must be small to increase the precision around the boundary between water and sand. The size of the elements at that fictive boundary is $\Delta x = 5$ [mm]. Then the size of the elements increases with the distance to the fictive line.
2. Close to the nozzle, delimited by the two red dots on the zoomed part of the mesh, the elements must also be small. It is indeed necessary for the simulations to have at least two elements at that boundary, since the velocity change is high. The size of the elements there is thus half the diameter of the nozzle: $\Delta x = \frac{1}{2} D_{jets} = 0.25$ [mm]. Then the size of the elements increases with the distance to the nozzle.

The final mesh is a combination of those two conditions, taking the minimum sizes between the two. The largest triangle has a size of about 4 [cm].

For every simulation, the initial conditions are the following:

- Boundary conditions as specified on figure 3.2;
- Horizontal velocity equal to U_0 at every node in the domain;
- Vertical velocity null at every node in the domain;
- Concentration as specified on figure 3.4. The concentration of water at the bottom layer is null, meaning that it is only pure sand. At the top layer, the concentration of water is 1, meaning that there is no sand present. The separation follows as close as possible the fictive line of the mesh, but being dependent on the boundaries of each elements.

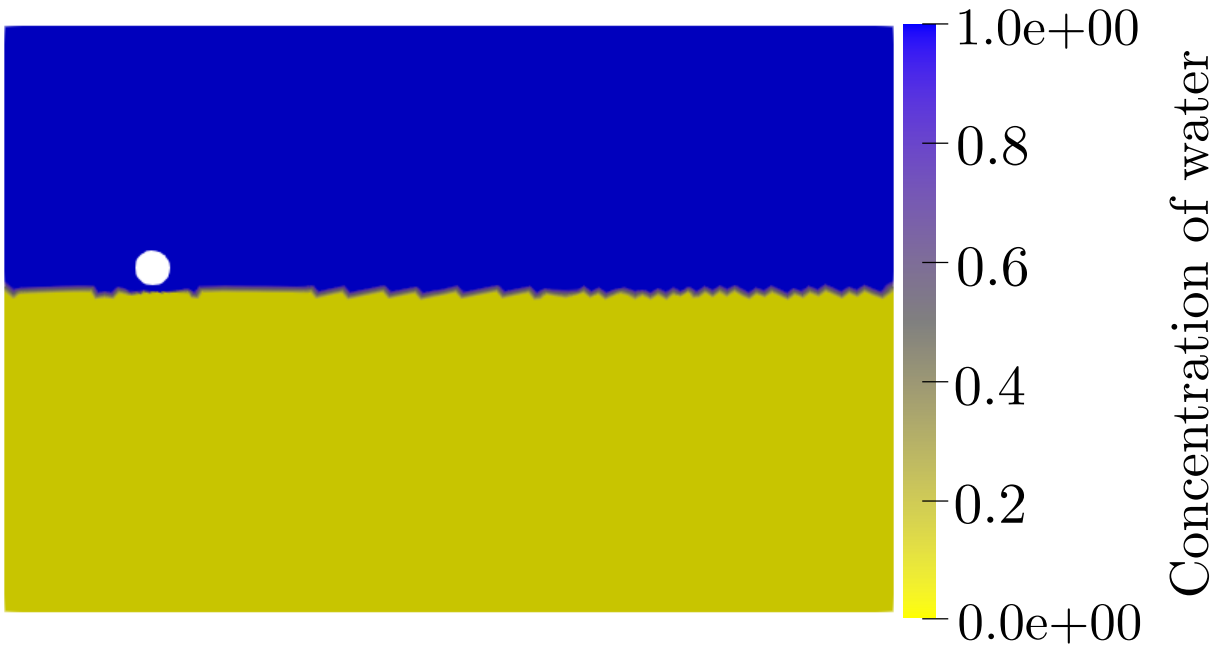

Figure 3.4: Concentration of water at time $t = 0$ [s]

3.2 Stability analysis

When solving the equations with numerical methods, the stability of the simulation is a very important matter. If the solving is unstable, the computational time will blow up and lead to wrong and unstable results. This section is thus focused on the stability analysis that determines the time step depending on the spatial step and on other parameters to obtain stable simulations.

The Courant–Friedrichs–Lewy number, β, is an important dimensionless number to ensure the stability of the schemes used to solve the equations, and is defined by equation 3.2.

$$\beta = \frac{U\Delta t}{\Delta x} \tag{3.2}$$

Where U is a representative velocity of the flow, Δt is the time step used in the simulation and Δx is the representative size of the mesh used. The stability condition is $\beta \leq 1$ since Migflow solves the equations in an explicit way.

Therefore, the critical values for U and Δx are the ones that increase the CFL number. The critical value for U is the highest velocity in the domain, the velocity V at the nozzle, given by equation 3.1. The critical value for Δx is the size of the smallest element, at the nozzle. Those values dictates the highest order possible of the time step, since it must compensate to obtain a final CFL number below 1.

Replacing those values in the equation, the CFL number can be expressed by equation 3.3.

$$\beta = \frac{2Q\Delta t}{BD_{jets}^2} \tag{3.3}$$

To estimate the order of the time step Δt, equation 3.3 is used. The different variables are:

- The flux. The maximum value for the flux is 122 $[\mathrm{mL\,s^{-1}}] = 122 \times 10^{-6}$ $[\mathrm{m^3\,s^{-1}}]$. It is thus of the order $\mathcal{O}(10^{-4})$ $[\mathrm{m^3\,s^{-1}}]$.
- The width of the tank. Its value is 12.6 [cm]. It is thus of the order $\mathcal{O}(10^{-1})$ [m].
- The diameter of the jet. Its value is 0.5 [mm]. It is thus of the order $\mathcal{O}(10^{-4})$ [m].

To have a CFL number of the order $\mathcal{O}(1)$, the time step must be of the order $\mathcal{O}(10^{-5})$ [s], a very restrictive and small value.

This restriction comes not only from the parameters close to the jet, but also from the schemes used to solve the concentration equation. Therefore, a bigger time step could be applied, and used to solve the Navier-Stokes equations. To solve the concentration equation, sub-iterations can be used to reduce the time step and keep the computations stable. With that method, the time step can be increased until the gain in processing time is not comparable to the gain in time step.

Furthermore, to see the dependence of the simulations to the time step, a test has been carried out, with the value for the parameters as shown in table 3.1 and two different Δt.

Figure	Q $[\mathrm{mL\,s^{-1}}]$	U_0 $[\mathrm{cm\,s^{-1}}]$	ν_{sand} $[\mathrm{m^2\,s^{-1}}]$	κ $[\mathrm{m^2\,s^{-1}}]$	C $[-]$	Z [mm]
3.5, 3.6	122	6.8	10^{-4}	10^{-5}	10^{-3}	5

Table 3.1: Parameters for the different simulations

The results are shown figure 3.5. The figure represents the concentration of the water on a part of the mesh, at a certain time t. It is apparent that the value of the concentration of water varies with the value of the time step.

To better understand what is shown on figure 3.5, the velocity magnitude is presented figure 3.6. It shows the influence of the jet on the formation of the small sand hills, downstream of the jet.

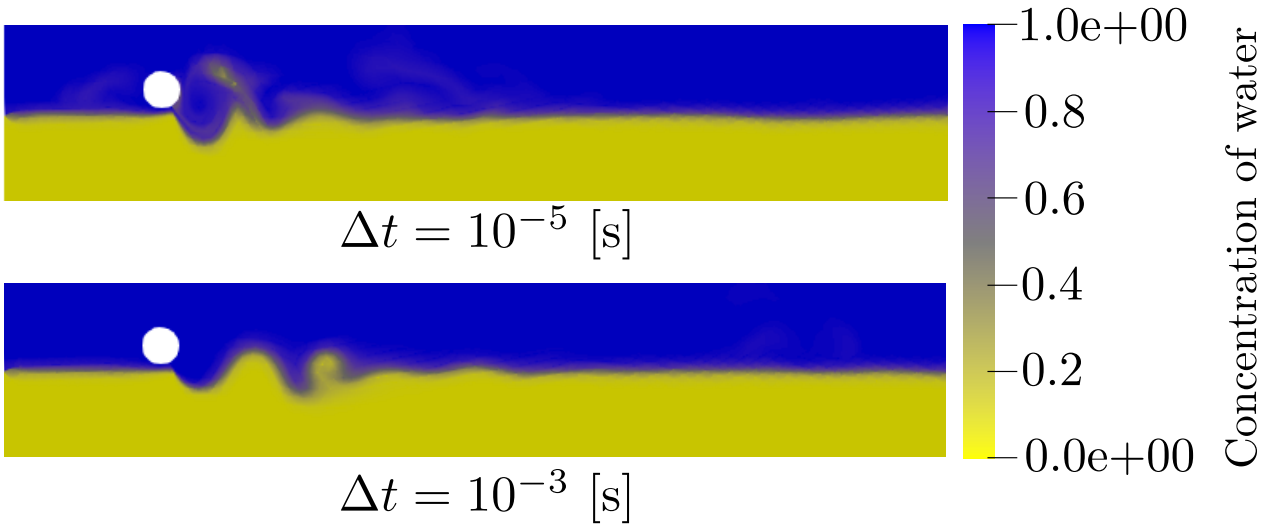

Figure 3.5: Concentration - different Δt at $t = 5$ [s]

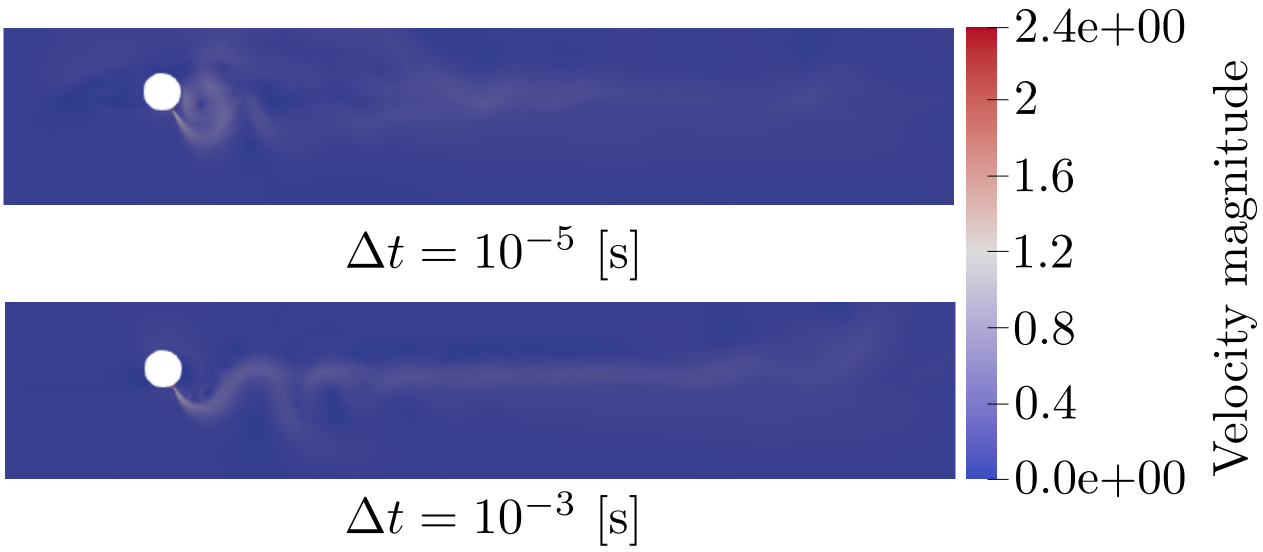

Figure 3.6: Velocity magnitude - different Δt at $t = 5$ [s]

In conclusion, the choice of the time step influences the results. The higher value for the time step is chosen here, to reduce the computational time. This implies that the results are thus not precisely representative of the reality and it is one reason why the simulations will not give the exact same results as the laboratory experiments.

3.3 Influencing parameters

Several parameters can influence the result of the different simulations and will be discussed in this section. The goal is to observe the impact of every parameter on the behaviour of the fluids and on the trench created and to discuss the consequences. When the effect of the parameters is understood, simulations are presented that look at the impact of the velocity of the vehicle and the jetting strength. Those results are also compared to the results obtained with the laboratory experiments. Each figure gives the concentration at a certain time t along with the streamlines of the flow, in black.

3.3.1 The kinematic viscosity of the sand ν_{sand}

The sand is approximated by a Newtonian fluid. Its kinematic viscosity is chosen so that its behaviour gets closer to the one of sand, a non-Newtonian fluid. The expectations are that the viscosity of the sand should be higher than the one of the water. The kinematic viscosity impacts the mixing of the sand with water. Increasing the viscosity should decrease the mixing and thus decrease the dimensions of the trench created. The following simulations are made without the sedimentation velocity and without mass dissipation, to see only the influence of the kinematic viscosity of the sand. The data for each simulation is given table 3.2. The simulations are not in stationary state, the time $t = 6$ [s] is chosen only to illustrate the influence of the kinematic viscosity at a certain time. This last remark is valid for all following simulations.

Figures	Q [mL s^{-1}]	U_0 [cm s^{-1}]	κ [m^2 s^{-1}]	C [–]	Z [mm]
3.7, 3.8, 3.9, 3.10, 3.11	107	6.8	0	0	5

Table 3.2: Viscosity of sand: parameters for the different simulations

First, figure 3.7 shows the result if the sand and the water would have the same viscosity. As expected, the boundary between the water and the sand is too disturbed and the sand behaves too much like water. In such a simulation, it is difficult for a trench to be created, since the sand and the water constantly mix together. Looking at the streamline, the influence of the jet has a big impact on a large part of the domain. This proves that the viscosity of the sand should be higher.

Then, the viscosity of the sand is multiplied by 10 on figure 3.8. The boundary is still too disturbed and a trench starts to be created but there is still too much mixing between the sand and the water and a large impact on the streamlines.

Increasing the viscosity of the sand by a factor of 10 again, figure 3.9 is obtained. The boundary between water and sand is not too disturbed, there is a good suspension of the sand and a trench is created. The streamlines show that the flow far from the jet is not impacted by it.

Finally, the viscosity of the sand is increased by a final factor of 10 to obtain figure 3.10, the sand layer is barely disturbed by the jet and a small trench is created. There is almost no suspension of sand. In this simulation, the viscosity of the sand is too high and it does not mix with water because of that. The flux out of the jet would have to be higher to dig a bigger trench. The streamlines are barely influenced by the presence of the jet. This shows that, even though the viscosity of sand should be higher than the one of the water, its value should not be too high.

A graph to compare all these simulations is given figure 3.11. It represents the boundary between sand and water, when there is as much sand as water, thus when $a = 0.5$. It illustrates the high mixing of sand with water when the viscosity is too low. On the figure, the difference between the depth of the trench at $\nu = 10^{-3}$ [m^2 s^{-1}] and the other cases is non negligible, the former being the less deep.

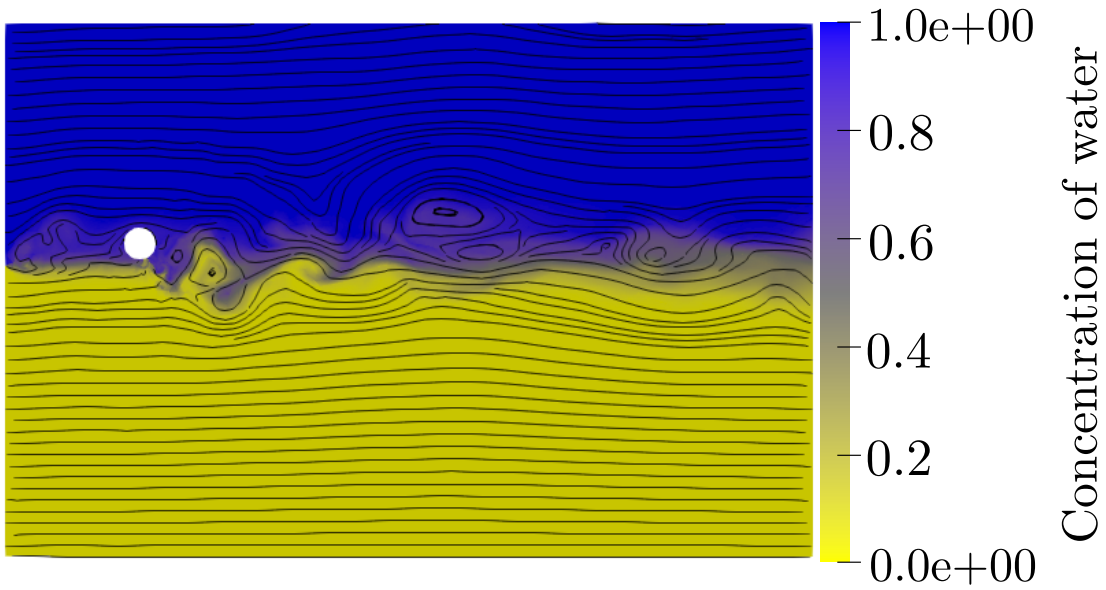

Figure 3.7: Viscosity of sand: $\nu_{sand} = \nu_{water} = 10^{-6}$ [$\mathrm{m}^2\,\mathrm{s}^{-1}$] at $t = 6$ [s]

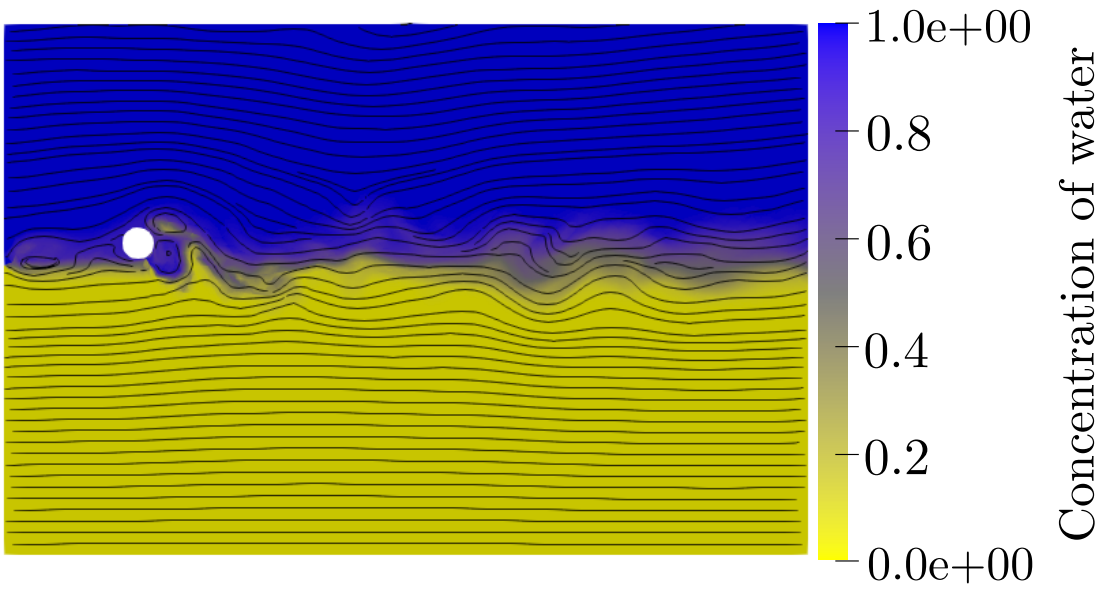

Figure 3.8: Viscosity of sand: $\nu_{sand} = 10^{-5}$ [$\mathrm{m}^2\,\mathrm{s}^{-1}$] at $t = 6$ [s]

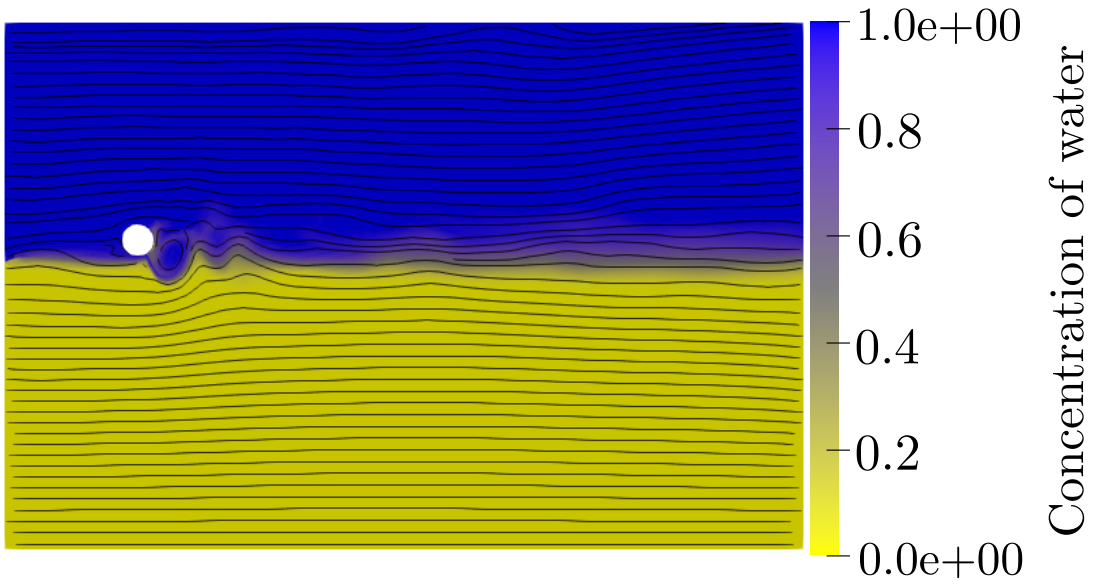

Figure 3.9: Viscosity of sand: $\nu_{sand} = 10^{-4}$ [$\mathrm{m}^2\,\mathrm{s}^{-1}$] at $t = 6$ [s]

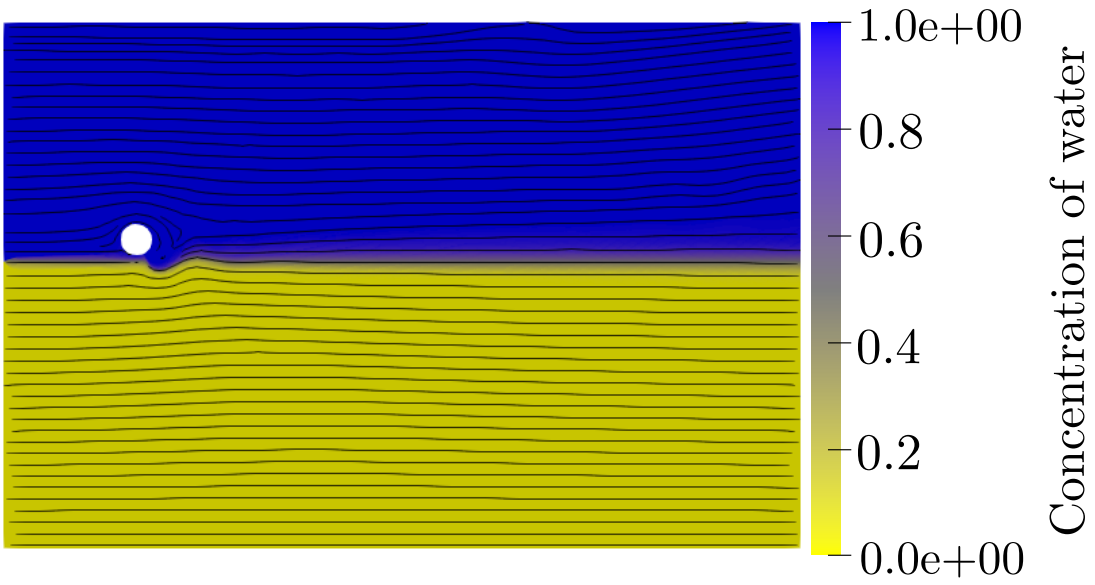

Figure 3.10: Viscosity of sand: $\nu_{sand} = 10^{-3}$ [$\mathrm{m}^2\,\mathrm{s}^{-1}$] at $t = 6$ [s]

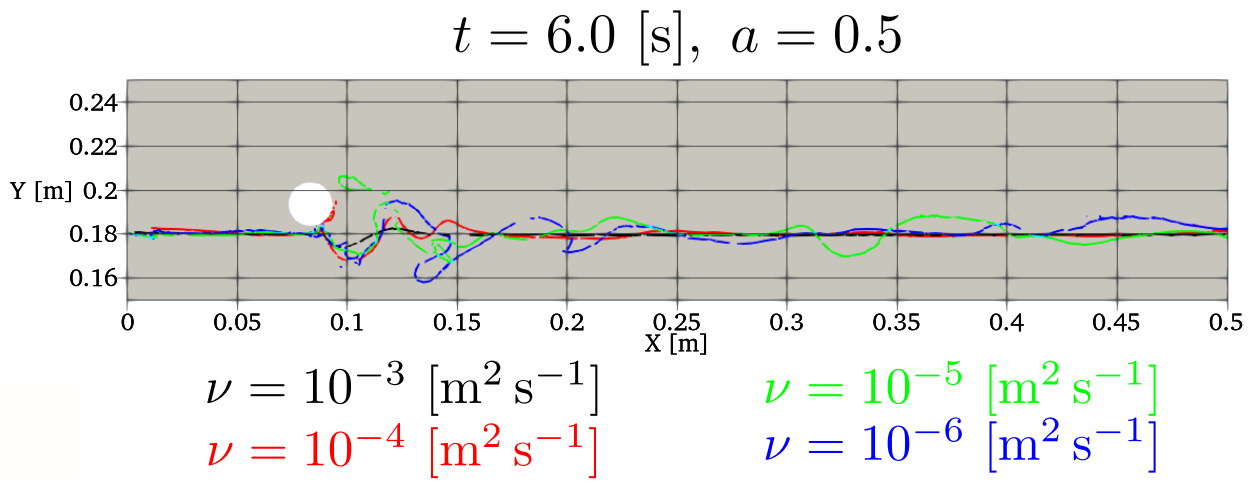

Figure 3.11: Viscosity of sand: comparison

3.3.2 The sedimentation coefficient C

The sedimentation velocity influences the rate of settling of the sand and its suspension. The value expected for the sedimentation coefficient is, on the one hand, not too low, or the sand would never settle on the floor and the cable would never be buried. On the other hand, if the value is too high, the sand would not go in suspension and the cable would again not be buried. The following simulations are made without dissipation, to see only the influence of the sedimentation coefficient. The data for each simulation is given table 3.3.

Figures	Q [mL s^{-1}]	U_0 [cm s^{-1}]	ν_{sand} [m^2 s^{-1}]	κ [m^2 s^{-1}]	Z [mm]
3.12, 3.13, 3.14, 3.15, 3.16	107	6.8	10^{-4}	0	5

Table 3.3: Coefficient of sedimentation: parameters for the different simulations

First, figure 3.12 is a simulation with a very low coefficient of sedimentation. The suspension is barely influenced, when comparing the result to figure 3.9, a simulation with the same input parameters except that there is no sedimentation. Downstream and far from the jet, the sand is still in high suspension, showing that the cable would not be buried in such a situation. For the cable to be buried, more sedimentation is needed.

Therefore, the coefficient of sedimentation is multiplied by 10 on figure 3.13. The sand goes in suspension and the thickness of suspended sand at the water-sand boundary is still high.

Then, on figure 3.14, the coefficient is once again increased by a factor of 10. The sand goes less in suspension and the thickness of suspended sand is lower than the previous simulation. This simulation is already closer to the expectations and to reality.

Finally, multiplying one last time the coefficient by 10, figure 3.15 is obtained. The sand does not go noticeably in suspension and the trench dug is free of suspended sand. This means that the cable would just lay in open water.

A comparison between all test cases has been made figure 3.16 and illustrates the suspension of sand at $a = 0.5$. There is only a small difference between all test cases, looking at the graph. The smaller the coefficient, the bigger the disturbance in the flow.

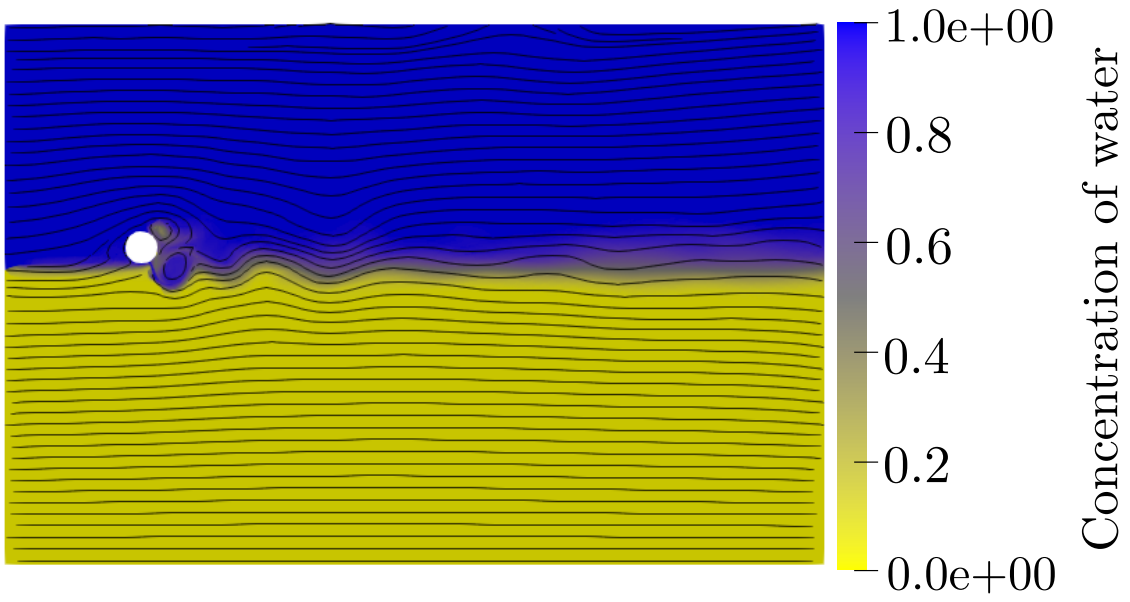

Figure 3.12: Coefficient of sedimentation: $C = 10^{-5}$ at $t = 6$ [s]

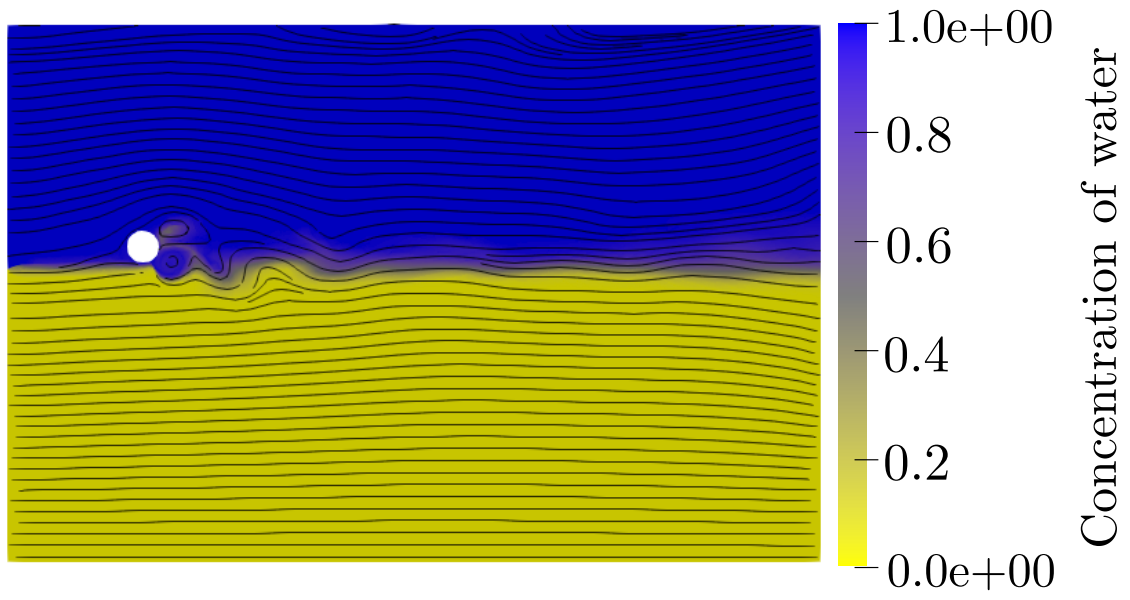

Figure 3.13: Coefficient of sedimentation: $C = 10^{-4}$ at $t = 6$ [s]

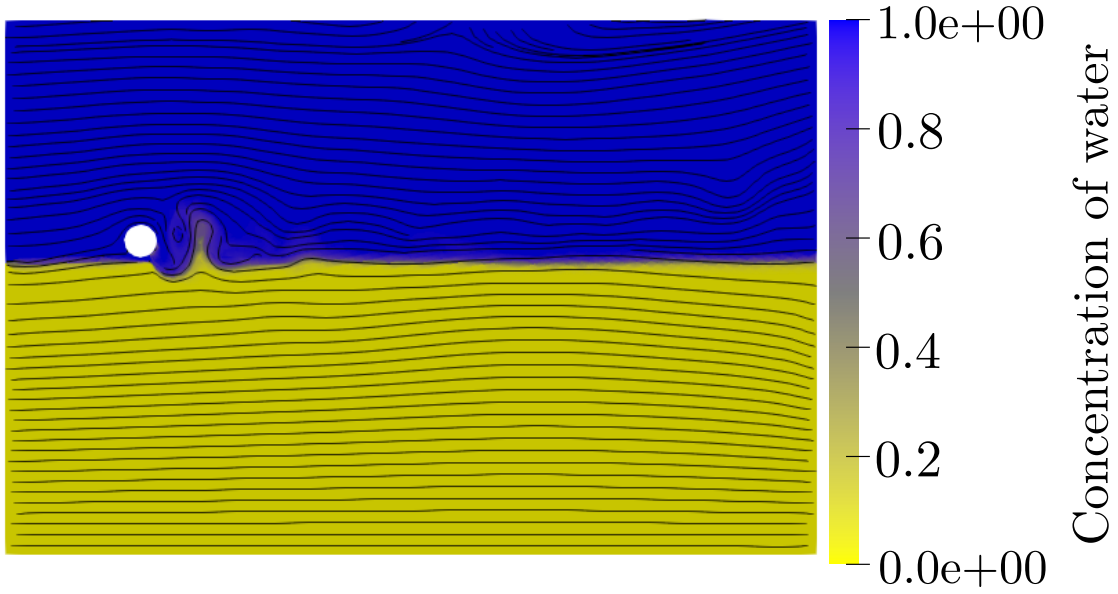

Figure 3.14: Coefficient of sedimentation: $C = 10^{-3}$ at $t = 6$ [s]

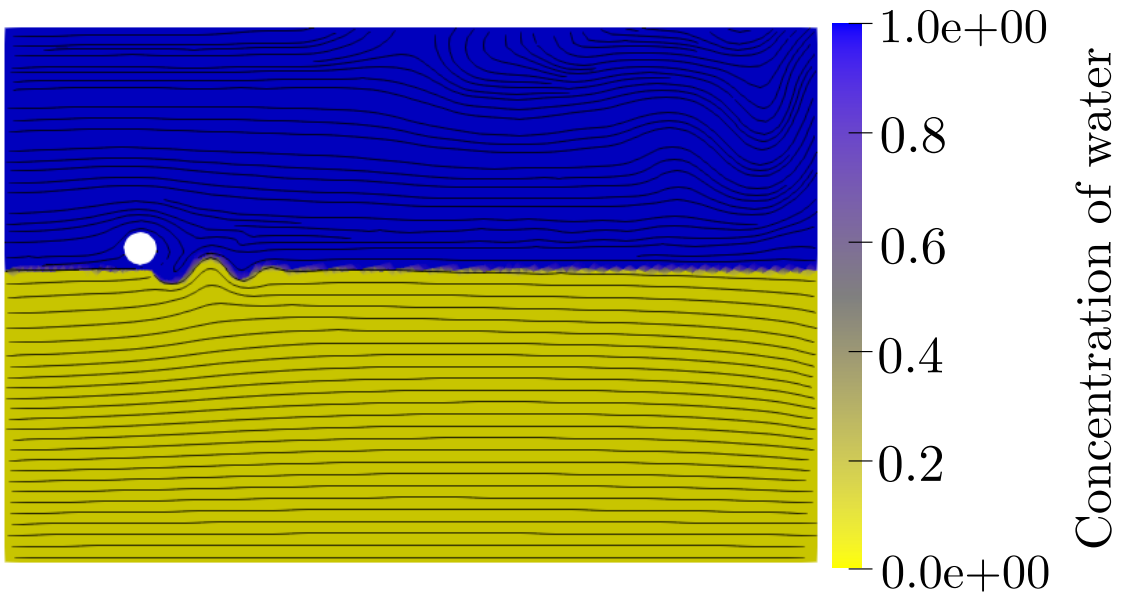

Figure 3.15: Coefficient of sedimentation: $C = 10^{-2}$ at $t = 6$ [s]

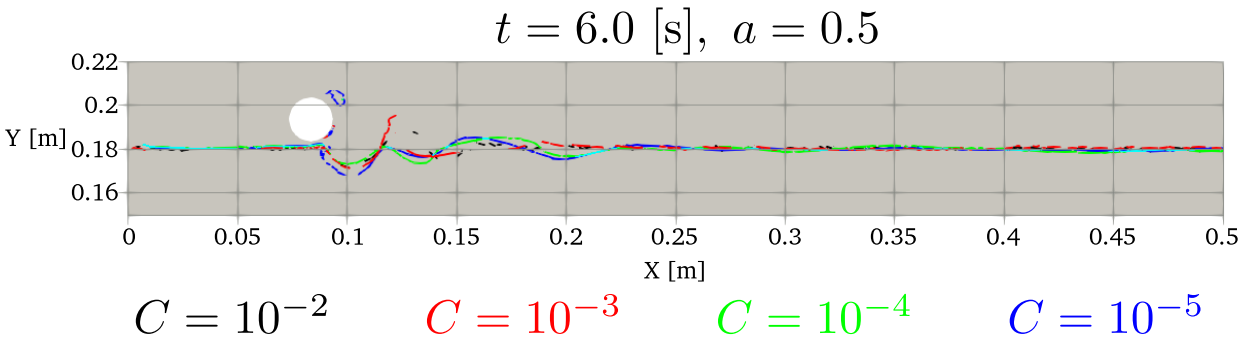

Figure 3.16: Coefficient of sedimentation: comparison

3.3.3 The mass diffusion coefficient κ

The mass diffusion coefficient influences the suspension of the sand in the water, as well as the mixing of the sand with water close to the jet. On the one hand, if its value is too high, the suspension layer would be too thick and would be unrealistic. On the other hand, if its value is too low, the boundary between the sand and the water would follow the border of the elements, as in figure 3.4, and would be unrealistic too. The following simulations are made without sedimentation, to see only the dependence of the mass diffusion coefficient on the thickness of suspension of the sand. The data for each simulation is given table 3.4.

Figures	Q [mL s^{-1}]	U_0 [cm s^{-1}]	ν_{sand} [m^2 s^{-1}]	C [–]	Z [mm]
3.17, 3.18	107	6.8	10^{-4}	0	5

Table 3.4: Mass diffusion coefficient: parameters for the different simulations

First, on figure 3.17, the value of the coefficient is 10^{-5} [m^2 s^{-1}]. The suspension of the sand is already present with such a small value.

Second, on figure 3.18, the value is increased by a factor of 10. The difference between the two simulations is very noticeable, meaning that the value of the coefficient of mass diffusion is sensitive. Here, the suspension layer is very thick.

The thicker the suspension layer, the higher the coefficient of sedimentation needs to be, to compensate and make it still realistic. To illustrate this, figure 3.19 presents three cases with different mass diffusion coefficients and different sedimentation coefficients. The figures are a zoom focused to the interesting part of the domain, the boundary between the water and the sand, to better compare the differences. The data for the three simulations is described table 3.5.

Figures	Q [mL s^{-1}]	U_0 [cm s^{-1}]	ν_{sand} [m^2 s^{-1}]	κ [m^2 s^{-1}]	C [–]	Z [mm]
3.19a	107	6.8	10^{-4}	10^{-4}	10^{-2}	5
3.19b	107	6.8	10^{-4}	10^{-4}	10^{-3}	5
3.19c	107	6.8	10^{-4}	10^{-5}	10^{-4}	5

Table 3.5: Mass diffusion and sedimentation coefficients: parameters for the different simulations

On the first simulation, figure 3.19a, the sedimentation is too strong compared to the mass diffusion. The last two results differ in both coefficient of sedimentation and in coefficient of mass diffusion, but the result is approximately the same. This shows that both coefficients compensate each other and several combinations lead to approximately the same results.

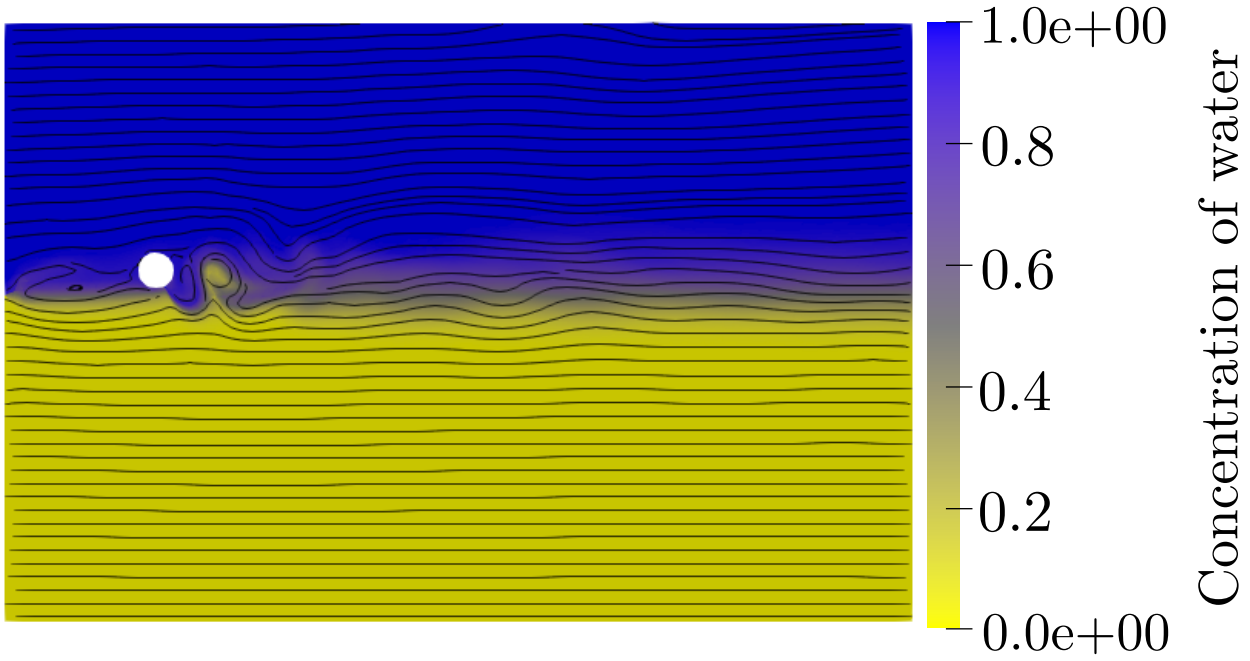

Figure 3.17: Mass diffusion coefficient: $\kappa = 10^{-5}$ [$\mathrm{m}^2\,\mathrm{s}^{-1}$] at $t = 6$ [s]

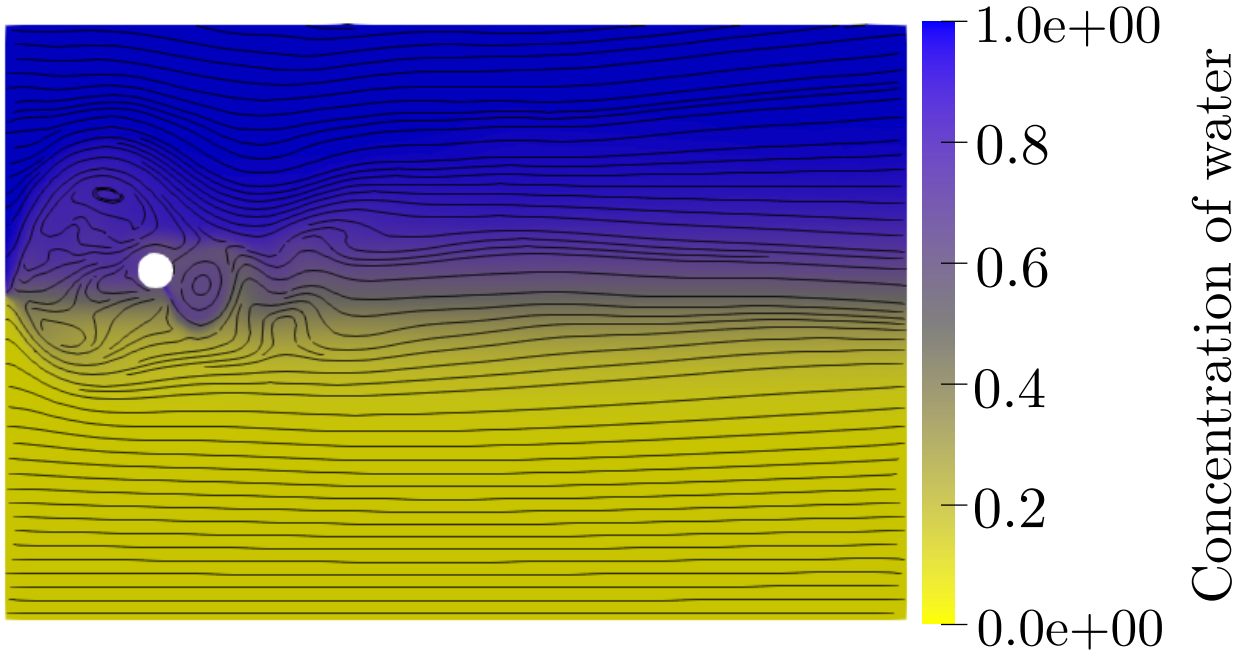

Figure 3.18: Mass diffusion coefficient: $\kappa = 10^{-4}$ [$\mathrm{m}^2\,\mathrm{s}^{-1}$] at $t = 6$ [s]

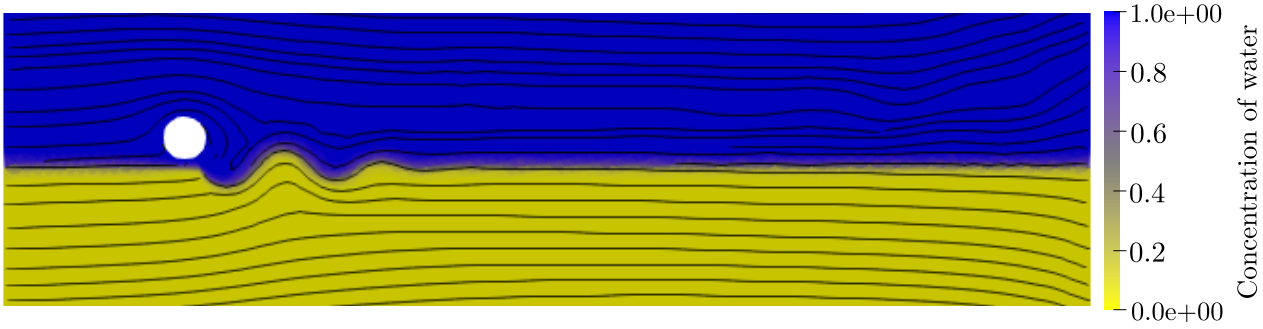

(a) $\kappa = 10^{-4}$ [m^2 s^{-1}], $C = 10^{-2}$ at $t = 6$ [s]

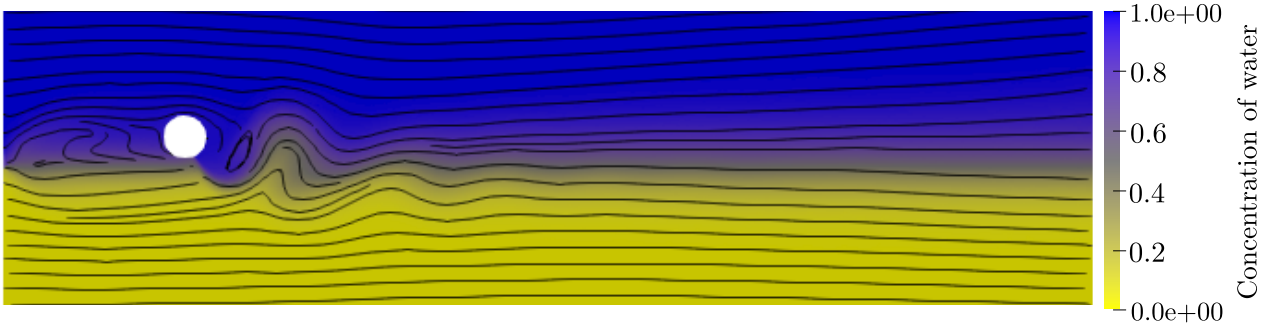

(b) $\kappa = 10^{-4}$ [m^2 s^{-1}], $C = 10^{-3}$ at $t = 6$ [s]

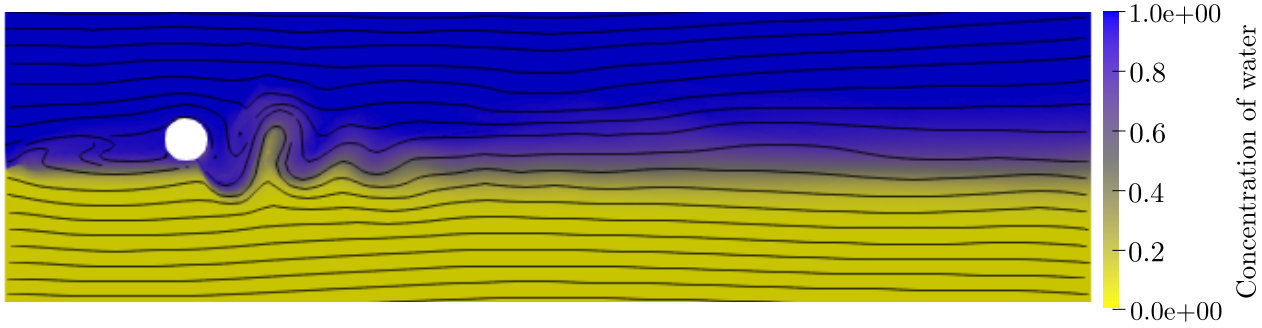

(c) $\kappa = 10^{-5}$ [m^2 s^{-1}], $C = 10^{-4}$ at $t = 6$ [s]

Figure 3.19: Variation of the mass diffusion and the sedimentation coefficients

3.3.4 The height of the jet Z

One idea to make the trench deeper in the simulations was to modify the height Z of the jet. The reflection was that if the jet is closer to the sand, its impact on the formation of the trench would be higher. Two simulations have been made, one with the standard height of jet, given in the article, and the other one reducing Z by more than half its standard value. A comparison between those two simulations has been made figure 3.20 and illustrates the suspension of sand at $a = 0.5$. The data for each simulation is given table 3.6.

Figures	Q [mL s^{-1}]	U_0 [cm s^{-1}]	ν_{sand} [m^2 s^{-1}]	κ [m^2 s^{-1}]	C [–]
3.20	107	6.8	5×10^{-4}	10^{-5}	5×10^{-4}

Table 3.6: Height of the jet: parameters for the different simulations

The difference between the two simulations is small, leading to the conclusion that reducing the height of the jets does not significantly influence the result. For the rest of the simulations, the standard value of the height of the jet, used in the article, will be used.

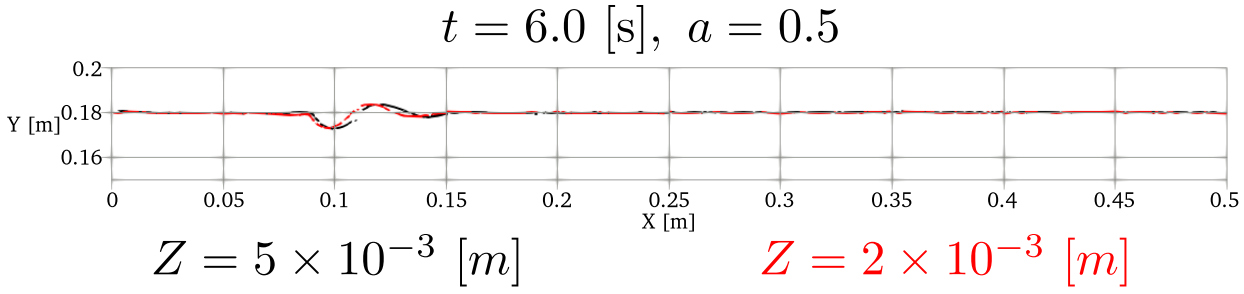

Figure 3.20: Height of the jet: comparison

3.3.5 The velocity of the ROV U_0

The velocity of the vehicle influences the shape of the trench and the suspension of the sand, since it determines the amount of time the jet is above a certain area of the ground. The expectations are that the lower the velocity U_0, the shorter the length of the trench. It should also influence the mixing of the sand in the water, close to the jet. Increasing the vehicle velocity should decrease that mixing. The following simulations are made as an attempt to reproduce the results of the experiments of Perng and Capart, using the analysis of the parameters made in the previous subsections. The data for each simulation is given table 3.7.

Figures	Q [mL s^{-1}]	ν_{sand} [m^2 s^{-1}]	κ [m^2 s^{-1}]	C [–]	Z [mm]
3.21, 3.22	107	10^{-4}	10^{-5}	10^{-3}	5

Table 3.7: Velocity of the ROV: parameters for the different simulations

First, three different velocities have been tested and the result is given figure 3.21. A comparison between all test cases has been made figure 3.22 and illustrates the suspension of sand at $a = 0.5$. It shows that increasing the velocity of the vehicle increases the length of the trench, but the depth is not noticeably influenced.

The figure 3.21a gives the result if the vehicle is not moving. That result can be compared to figure 3.23, image (a), that shows the result of the experiment in the same situation. In the experiment, the mixing close to the jet is very high and small hills of sand on both sides of the vehicle are forming. In the simulation, that mixing is also present but with a lower intensity and no hill is present.

The figure 3.21b gives the result if the vehicle is moving slowly. That result can be compared to figure 3.23, image (c), that shows the experiment result in approximately the same situation. In the experiment, the shape of the trench is different than on image (a), more elongated. The mixing of the sand with water is still high. In the numerical simulation, the shape of the trench is also different than in the first case, but the suspension of the sand is lower than in the experiment.

Finally, figure 3.21c gives the result if the vehicle is moving fast. That result can be compared to figure 3.23, image (d), that shows the experiment result in the same situation. In the experiment, the sand is barely in suspension and the trench is deep and long. In the simulation, if only looking at the first trench close to the jet, the result is very similar to the experiment. However, in the simulation, the sand behaves like a dissipating wave, downstream from the jet.

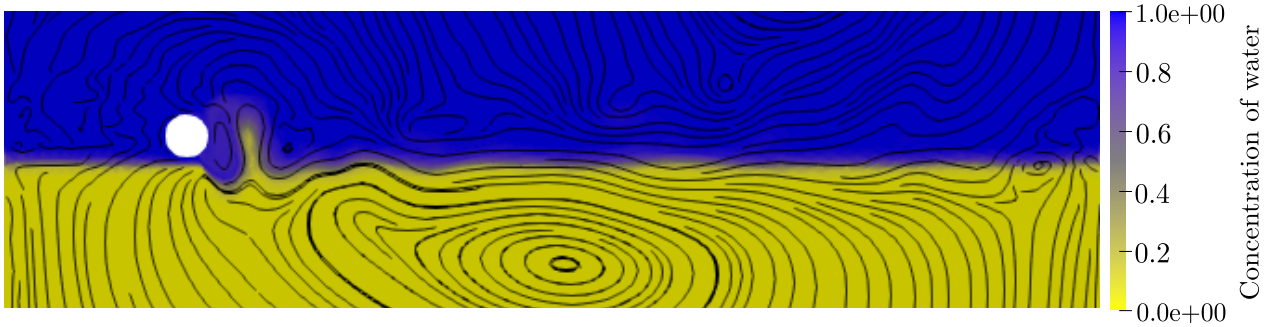

(a) $U_0 = 0$ [cm s^{-1}] at $t = 6$ [s]

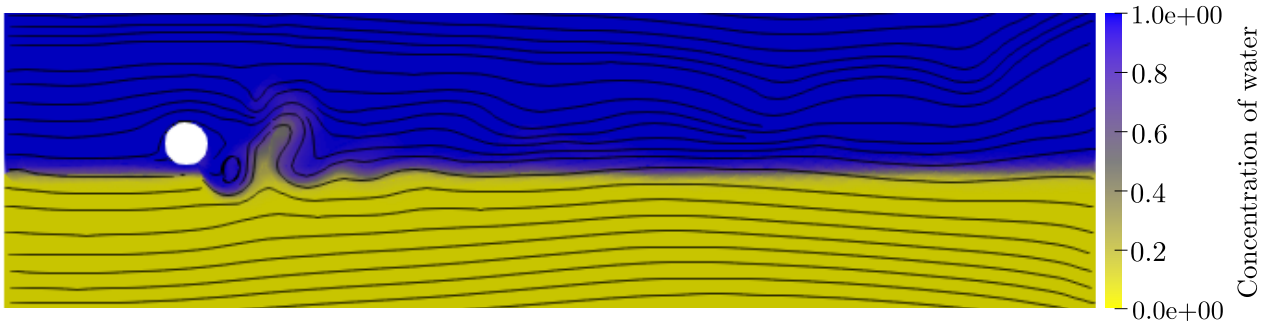

(b) $U_0 = 6.8$ [cm s^{-1}] at $t = 6$ [s]

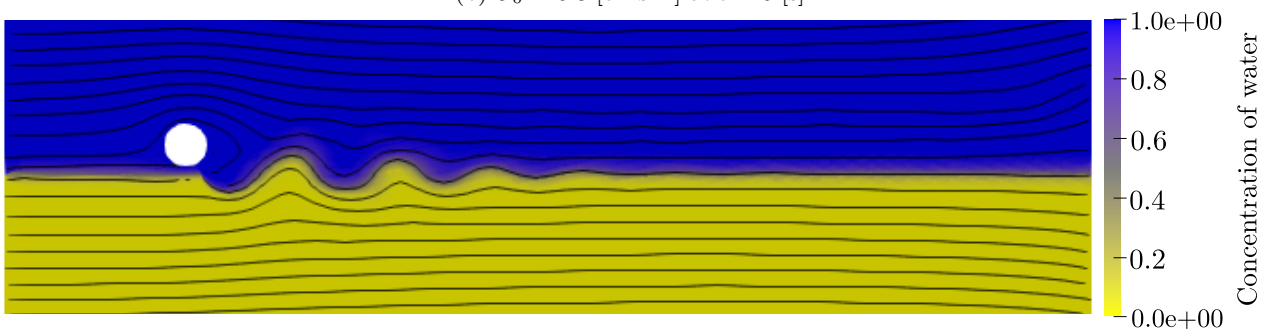

(c) $U_0 = 10$ [cm s^{-1}] at $t = 6$ [s]

Figure 3.21: Variation of the velocity of the ROV

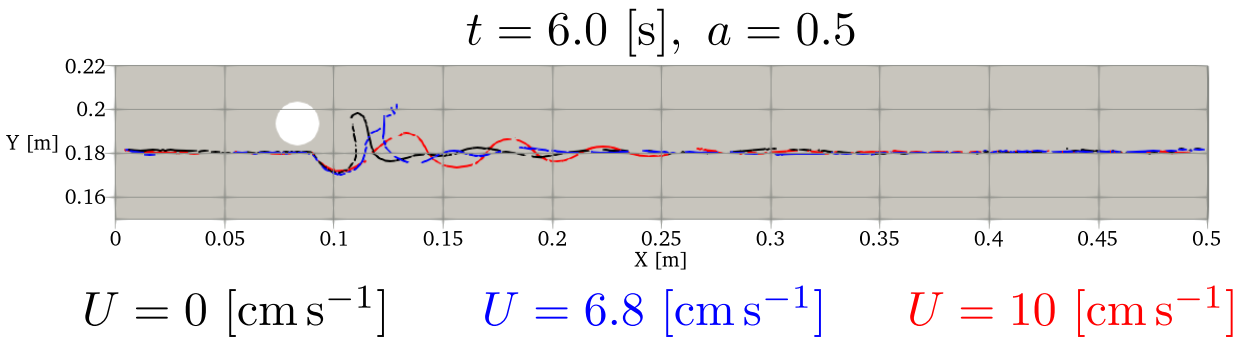

Figure 3.22: Velocity of the ROV: comparison

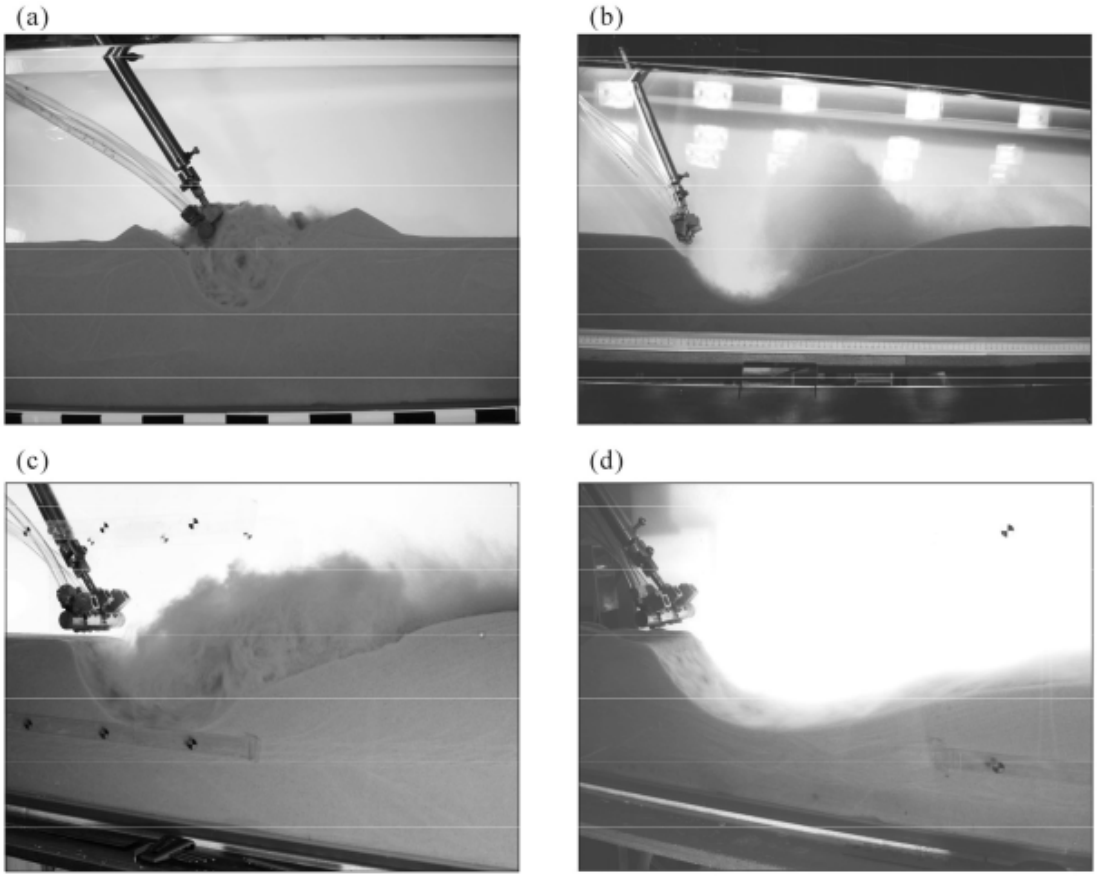

Figure 3.23: Results of the laboratory experiments, figure 5 in [1]

In the article, another comparison has been made, using graphs. The small-scale experiment has been realised at different velocities and the depth and length of the trench along with the suspension of the sand are shown on different graphs. Those graphs are shown here on figure 3.25. They are reproduced with Migflow to compare the results.

First, when observing the graphs of the experiment, several conclusions can be drawn. At low jetting strength, increasing the velocity of the vehicle does not noticeably influence the depth but it does influence the length of the trench. The depth of the trench is about 5 [cm] and the length varies between 20 and 30 [cm]. The suspension is also reduced when the velocity of the vehicle is increased.

Simulations have been run with the same flux and the same velocities, to compare with the laboratory experiment, and the result is shown figure 3.26. The data for those simulations is given table 3.8. The x-axis in the figure is not the same as in figure 3.25, where $\hat{x} = x + U_0 t$, but the scale and thus the difference between two x or $\hat{x}$ is the same. The y-axis is modified to be the same as in the experiment, with $y = 0$ at the level of the boundary between water and sand.

Figures	Q [mL s^{-1}]	ν_{sand} [m^2 s^{-1}]	κ [m^2 s^{-1}]	C [–]	Z [mm]
3.26	90	10^{-4}	10^{-5}	10^{-3}	5

Table 3.8: Velocity of the ROV: parameters for the different simulations

The results are not close to the experiment. First, the depth of the trench in the simulations reach 2 [cm] instead of 5 [cm]. The depth of the trench stays constant, as in the experiment. Then, the length of the trench varies only of a few centimetres and not of 10 centimetres as in the laboratory. Finally, the suspension does not decrease when the velocity increases. The main problem in the result is thus the depth of the trench and none of the parameters discussed above provides significant change to that depth to solve that problem.

One of the reasons for such a result is the model of the viscosity of the sand. In these simulations, the sand behaves as a Newtonian fluid, whatever the value of the viscosity chosen. This means that, due to the gravity effect, the sand layer will have a tendency to flatten out, reducing the depth of the trench created. In reality, gravity acts on the sand particles, but they will form a hill after the trench, whose slope will depend on the sheer stress. This could be solved using a model to imitates the non-Newtonian behaviour of sand. For example, the Bingham Plastic Model could be implemented [24]. With that model, the fluid does not flow until the sheer stress tops a certain critical value. In the simulations, this would force the sand to form hills and might solve the problem of depth and the other problems that are a consequence of that low depth. The difference of behaviour between Newtonian fluids and fluids represented by the Bingham Plastic Model is shown figure 3.24.

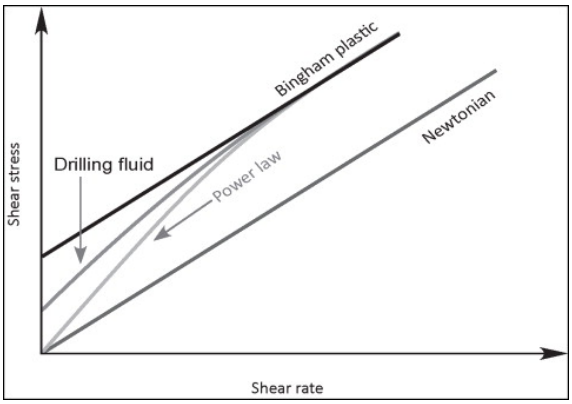

Figure 3.24: Illustration to differentiate Newtonian fluids model to Bingham Plastic model, taken from [24]

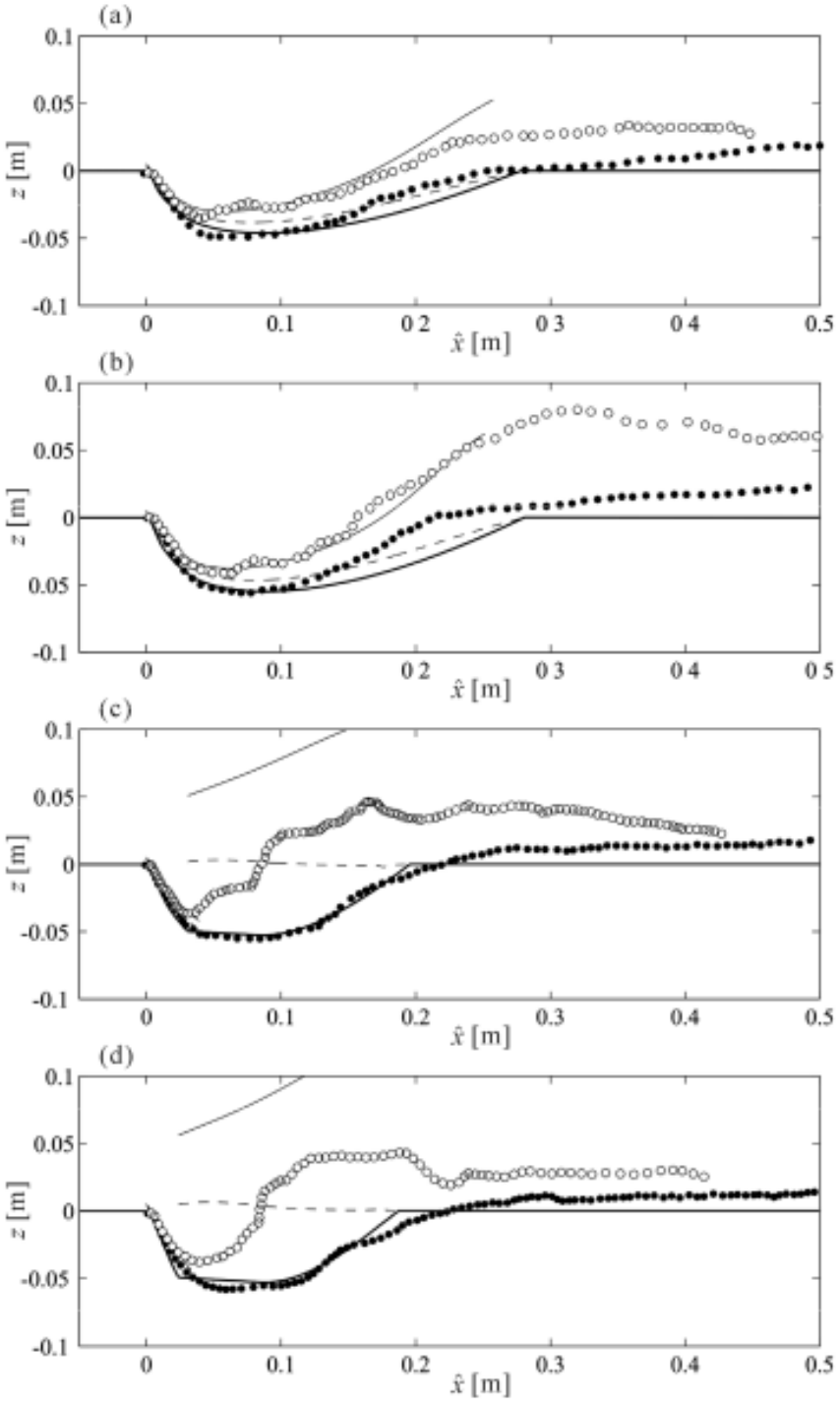

Figure 3.25: Results of the laboratory experiments, figure 12 in [1]. Filled circles = bed profile; hollow circles = outer line of the suspended sediment; curves = result of the sub-layered shallow flow theory. $Q = 90$ [mL s^{-1}]; (a) $U_0 = 4$ [cm s^{-1}]; (b) $U_0 = 3.5$ [cm s^{-1}]; (c) $U_0 = 2.9$ [cm s^{-1}]; (d) $U_0 = 2.4$ [cm s^{-1}]

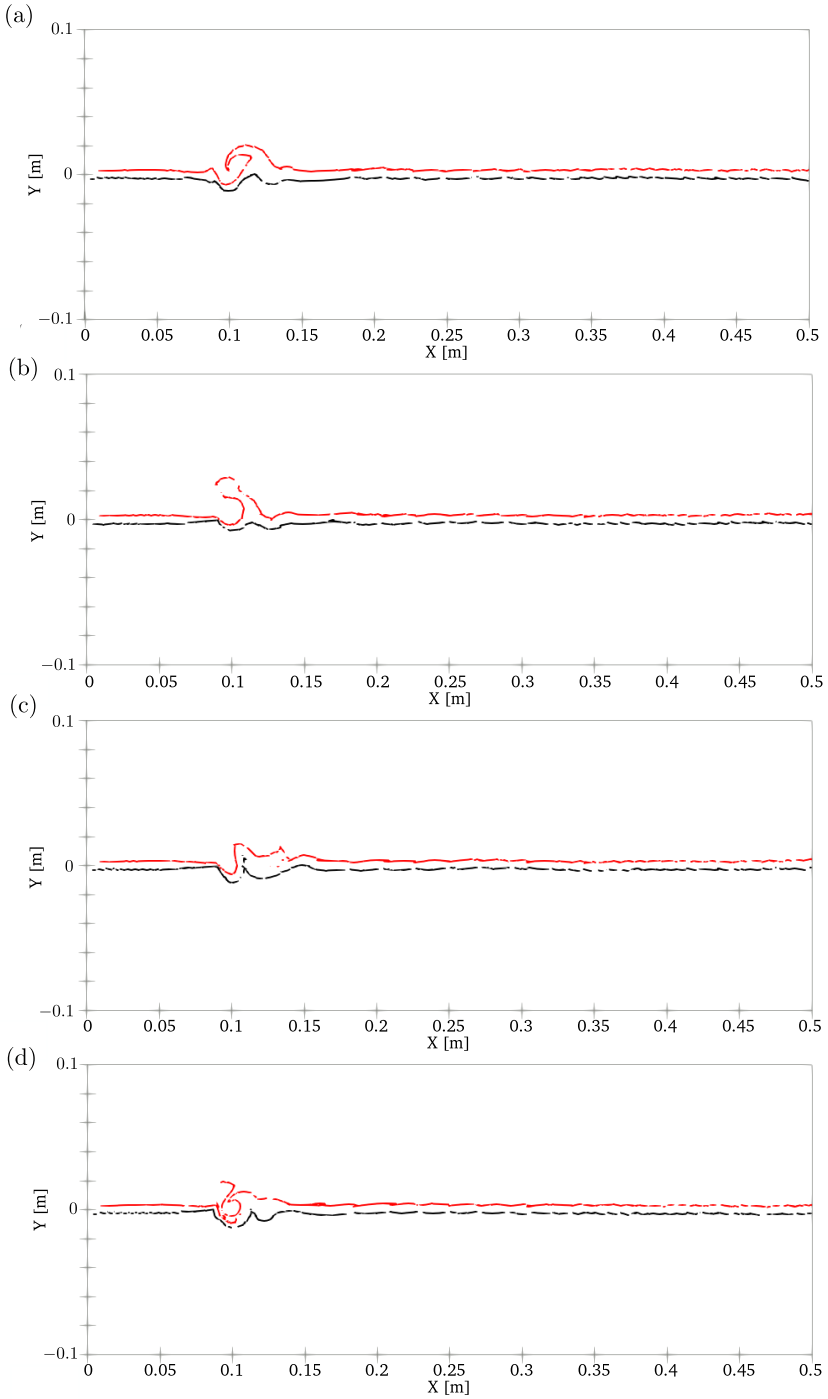

Figure 3.26: Results of the simulations. Black curve = bed profile; Red curve = outer line of the suspended sediment. $Q = 90$ [mL s^{-1}]; (a) $U_0 = 4$ [cm s^{-1}]; (b) $U_0 = 3.5$ [cm s^{-1}]; (c) $U_0 = 2.9$ [cm s^{-1}]; (d) $U_0 = 2.4$ [cm s^{-1}]

In conclusion, in the simulations, the velocity of the vehicle influences the length of the trench and the suspension of the sand. The higher the velocity, the longer the trench and the lower the suspension. Even though those conclusions match the predictions, the simulations are not perfect yet and do not reproduce exactly what has been experimented by A.T.H. Perng and H. Capart in their laboratory.

3.3.6 The flux at the jet Q

The flux at the jet influences the shape of the trench, since it is related to the jetting strength applied to the soil. In the laboratory experiments [1], the depth and the length of the trench are increased with the value of the flux. The higher the flux, the higher the suspension of sand in the water. The following simulations are again made as an attempt to reproduce those results. The data for each simulation is given table 3.9.

Figures	U_0 [$\mathrm{cm\,s^{-1}}$]	ν_{sand} [$\mathrm{m^2\,s^{-1}}$]	κ [$\mathrm{m^2\,s^{-1}}$]	C [–]	Z [mm]
3.27a, 3.27b, 3.27c, 3.28	6.8	10^{-4}	10^{-5}	10^{-3}	5

Table 3.9: Parameters for the different simulations

First, the lower value for the flux is used in the simulation, and the result is shown figure 3.27a. A zoom is made on the interesting part of the domain, to better see the trench created. The depth and the length of the trench are both small.

Then, the jetting strength is increased and the result is shown figure 3.27b. Comparatively to the previous image, the suspension of the sand is higher and the impact on the soil downstream is also higher. There is no clear influence on the depth or the length of the trench compared to the previous case.

Finally, the flux is at its highest value and the result is shown figure 3.27c. The length and the depth of the trench is increased when compared to the two previous simulations. The impact on the soil downstream is also increased.

A comparison between those simulations has been made figure 3.28 and illustrates the suspension of sand at $a = 0.5$. Increasing the flux increases thus the depth and the length of the trench, as observed on the graph and as predicted before. Increasing the jetting strength also increases the disturbance of the sand.

In summary, the behaviour predicted by the laboratory is found in the simulations, even though the simulations do not reproduce what is obtained in the experiment, as discussed in the previous subsection.

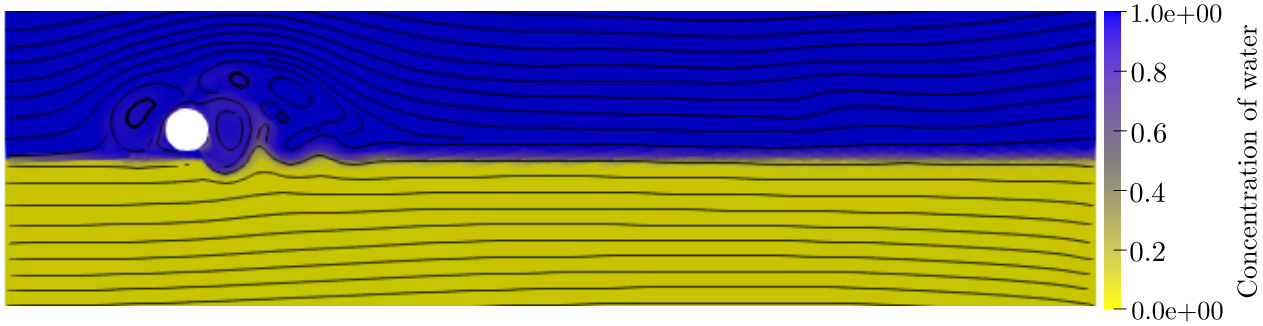

(a) $Q = 90$ [mL s^{-1}] at $t = 10$ [s]

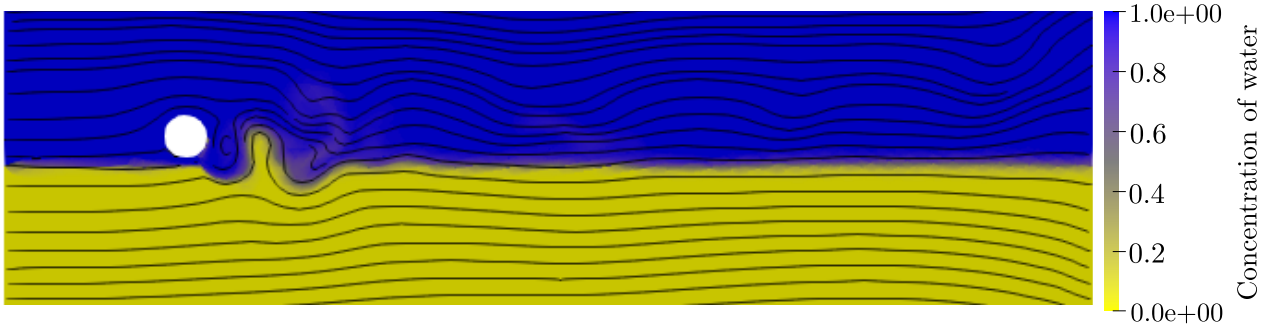

(b) $Q = 107$ [mL s^{-1}] at $t = 10$ [s]

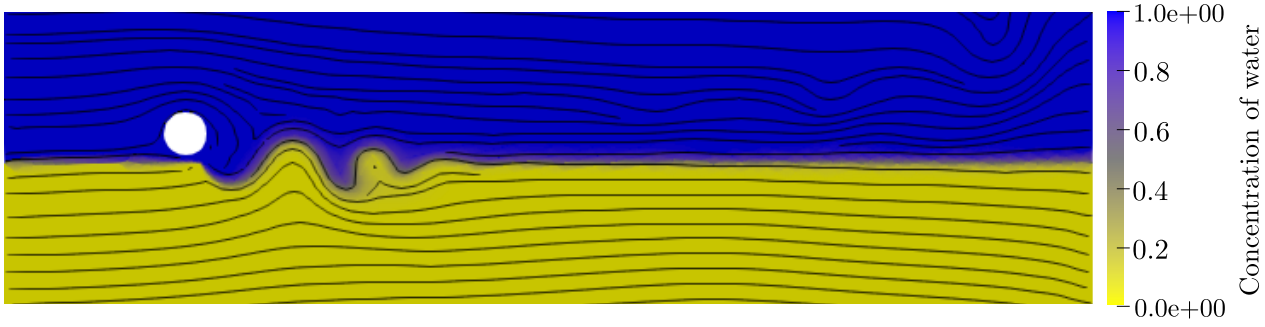

(c) $Q = 122$ [mL s^{-1}] at $t = 10$ [s]

Figure 3.27: Variation of the flux at the jet

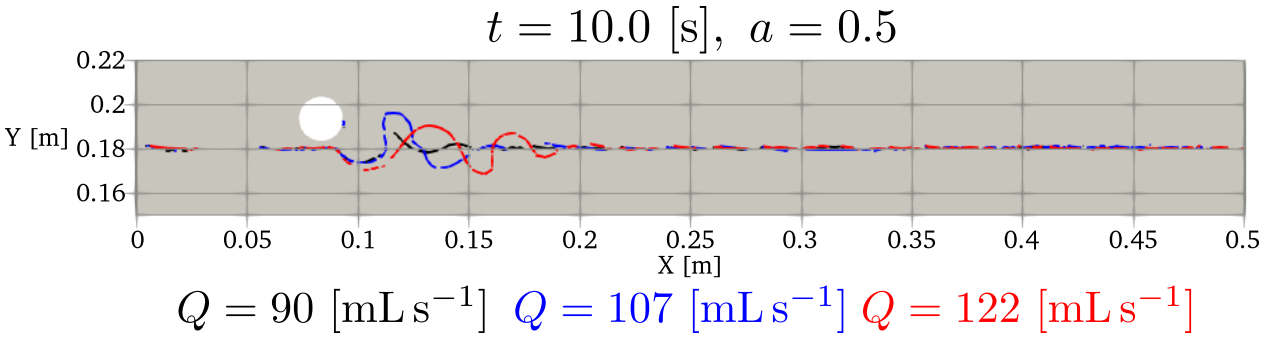

Figure 3.28: Flux at the jet: comparison

Chapter 4

Conclusion

Due to the emerging of the offshore industry, such as offshore wind farms, dredging is a method that has been evolving these past few decades. There exist mechanical and hydraulic dredgers and those differ by the way they extract the soil and dig trenches. Mechanical dredgers use a bucket to dig and collect the soil. Hydraulic dredgers use a pump and jets to form a trench. One example of a hydraulic dredging system is the remotely operated vehicle equipped with a jetting system. That vehicle is placed on the sea floor and deploys its sword, using the high pressure jets to dig in the soil. The sword is deployed at a certain angle from the vertical, chosen before the deployment of the machine. While the vehicle moves at constant velocity, the jets dig a trench of a certain depth and lay a cable in that trench. Low pressure jets are used downstream to maintain the soil in suspension. Due to the jets, the soil, sand for example, is suspended in the water and sedimentation takes place due to the action of gravity on the soil particles. This buries the cable underneath a layer of soil, at a certain depth, protecting it from external damage.

The goal of this thesis was to use computational fluid dynamics to recreate that situation and make a preliminary study of the impact of the velocity of the vehicle and the velocity at the jets on the geometry of the trench, such as the depth and the length. To achieve that, the software Migflow has been used and its code modified to fit the problem.

The jetting method has been experimented in laboratories in plenty of different studies and tested numerically in a few researches. One of those studies is the laboratory experiment led by A.T.H. Perng and H. Capart [1]. Their idea was to recreate a small-scale jetting system, in a tank filled with water and sand. The jetting system moved from one side of the tank to the other side, while jets of water created a trench. The velocity of the vehicle and the jetting strength were analysed in their study. They also developed a mathematical model to compute the shape of the trench, depending on the input parameters such as the horizontal velocity of the vehicle or the flux at the jets. The laboratory experiment provides different results, that were used in this thesis to compare with the results of the simulations.

A first step was to determine the different equations governing the problem. The general Navier-Stokes equations, along with the incompressibility condition, were already part of the software, averaged using the volume fraction of fluid compared to the volume fraction of grains. In this case, that volume fraction was unity and the equations returned to the basic Navier-Stokes equations. It was first tested on a simple jetting problem, with one fluid. The result being satisfying, the other equations could be developed. Next, an equation was needed to determine the variation of the concentration of water and of sand. This was needed since both have different properties and are mixed together due to the jets. That equation of concentration took two effects into account: the advection and the mass diffusion of concentration. To obtain correct results, the equation had to be developed and the incompressibility hypothesis had to be imposed, to obtain in the end the consistent version of the concentration equation. Finally, a study was needed to determine the velocity of sedimentation. This velocity gives the rate at which the sand settles on the ground due to the

gravity acting on each of its particles, or the rate at which the water gets cleared of the sand. The equation was first tested on a simple 1D problem, to see if the behaviour of both fluids lead to a correct result. Once that done, the velocity was introduced in the code of the software. Adding this velocity in the advection part of the equation of concentration brought a problem when computing the flux at the boundary between two elements. It was solved through trials and errors with simulations and with a reflection on the equation. There were two possibilities to compute that flux: using forward or backward differences, depending on where the information comes from. But those two options brought errors and a wrong behaviour for the settlement of the sand. The last idea was to combine forward and backward differences. For the sedimentation velocity, the information comes indeed from both directions. This idea could also be seen when looking at the equations and when using the method of characteristics to observe where to take the information. Implementing both forward and backward differences for that advection equation in the software gave the good behaviour, the sand settling correctly on the ground and the water getting pure, on top of the sand.

Now that the equations were known and correct, the setup of the laboratory experiment could be reproduced numerically. A definition of the domain and the mesh was given, with the differences between the numerical study and the laboratory setup. The boundaries and initial conditions were also detailed. Once the domain and the mesh defined, a stability analysis has been done to determine the time step needed for the simulation, using the Courant-Friedrichs-Lewy number. Due to the high velocity at the jet and low spatial step at the jet, the time step needed should be 10^{-5} [s] to obtain a CFL number lower than unity. But this condition applies only to the concentration equation, whose solving is more restrictive concerning the stability when done numerically. A bigger time step could be used, as long as sub-iterations were applied to solve that particular concentration equation. The time step used for the rest of the thesis was 10^{-3} [s]. However, it was discovered that changing the time step changes the simulations.

Furthermore, different tests have been carried out to see the impact of different variables on the simulations. The kinematic viscosity of the sand impacts the mixing of the sand with the water. The higher the value, the higher the jetting force needed to dig a trench. The lower the value, the higher the mixing and the more difficult to have a trench forming. Then, the sedimentation coefficient was analysed. It impacts the rate of settling of the sand and it represents the influence of gravity on the particles of sand. Its value should be low enough to have an elevation of the sand so it can bury the cable afterwards, with the action of gravity. However, the value should be high enough or the sand would never settle on the ground, because the impact of gravity on the suspended particles of sand is too low. A third parameter analysed was the mass diffusion coefficient. Its value determines the mass diffusion of the sand. It should be high enough for the border between sand and water to not follow the shape of the elements and be more realistic. On the other hand, it should be low enough or the mass diffusion is too high and the thickness of the boundary between pure water and pure sand would be too high. A comparison was then made to see the differences when changing the values of the mass diffusion and sedimentation coefficients. It was concluded that several different combinations of both coefficients can lead to the same results. A final parameter analysed was the height of the jet. The idea was to see if it influenced the depth of the trench, but it did not and the influence of that parameter was neglected.

Once those different parameters analysed, the velocity of the vehicle was tested. First, different values were tested to see the general change of behaviour in the simulations due to the increasing horizontal velocity. It showed that the length of the trench was increased and the suspension of the sand was decreased when the velocity of the vehicle was increased. It matched the predictions. Those results were compared to the experiments, and it showed a few differences between both situations. In the laboratory, the mixing of the sand was higher than in the simulations, and a small hill of sand was forming close to the trench, which was not the case in the simulations. Next, another comparison has been made, reproducing graphs of the sand bed and of the suspension of sand depending on the velocity of the vehicle, at fixed jetting strength. The results were different from the laboratory results. The depth of the trench was not deep enough and the change in the length of the trench was not high enough. The suspension of the sand was also not as impacted by the change of velocity as in the laboratory. One reason for those differences is the model used for the sand. It was approximated by a Newtonian fluid, with a constant viscosity. In reality, sand is a non-Newtonian

fluid and its viscosity should be modelled. The Bingham Plastic model could be used to mimic the behaviour of real sand. The final analysis made was the study of the flux at the jet. Three values have been used in the laboratory and thus tested in the simulations. It was predicted that the depth and the length of the trench would increase due to the increase of the flux. That behaviour was observed in the simulations.

In conclusion, the preliminary study of jet trenching using the software Migflow has to be improved to match the real results observed in laboratories. The sedimentation velocity is validated, as well as its implementation in the concentration equation. This concentration equation has been tested and confirmed on a simple 2D problem. Testing the simulations on the real domain showed that the results do not match the laboratory experiments. To obtain more realistic results, the viscosity of the sand should be modelled to have the behaviour of a non-Newtonian fluid, instead of a Newtonian fluid with a high viscosity. Another point to be studied more in depth is the stability of the simulations and the impact of the time step on the result. In this study, it has indeed been shown that different time steps give different results. Those are two ideas to continue this preliminary study and obtain results closer to the reality.

Bibliography

[1] A. T. H. Perng and H. Capart, "Underwater sand bed erosion and internal jump formation by travelling plane jets," Journal of Fluid Mechanics, vol. 595, pp. 1–43, Jan. 2008, publisher: Cambridge University Press. [Online]. Available: https://www.cambridge.org/core/journals/journal-of-fluid-mechanics/article/abs/underwater-sand-bed-erosion-and-internal-jump-formation-by-travelling-plane-jets/EEA5D9958012E24CAF5C5463670995C3

[2] A. C. Palmer and R. A. King, Subsea pipeline engineering. Tulsa, Okla.: PennWell Corporation, 2008, oCLC: 183179619.

[3] "EuDA - About dredging - Types of dredger." [Online]. Available: https://european-dredging.eu/Types_of_dredger

[4] K. J. Zanker and S. T. Bonnington, "9 Recent research developments In hydraulic dredging," in Dredging (1967 conf). Thomas Telford Publishing, Jan. 1968, pp. 81–87. [Online]. Available: https://www.icevirtuallibrary.com/doi/abs/10.1680/d1967c.44777.0012

[5] D. Knox, D. J. Krumholz, and J. E. Clausner, "Water Injection Dredging in the United States." ASCE, 1994, pp. 847–856. [Online]. Available: https://cedb.asce.org/CEDBsearch/record.jsp?dockey=0091198

[6] "Q1400 Trenching ROV." [Online]. Available: https://globaloffshore.co.uk/vessels-trenching-assets/q1400/

[7] "Global offshore and onshore geotechnical and survey services." [Online]. Available: https://www.fugro.com/

[8] P. G. Atangana Njock, Q. Zheng, N. Zhang, and Y.-S. Xu, "Perspective Review on Subsea Jet Trenching Technology and Modeling," Journal of Marine Science and Engineering, vol. 8, no. 6, p. 460, Jun. 2020, number: 6 Publisher: Multidisciplinary Digital Publishing Institute. [Online]. Available: https://www.mdpi.com/2077-1312/8/6/460

[9] H. Rouse, "Criteria for Similarity in the Transportation of Sediment," University of Iowa Studies in Engineering, vol. 20, pp. 33–49, 1940, conference Name: Hydraulics Conference Meeting Name: Hydraulics Conference Place: Iowa City, IA Publisher: State University of Iowa. [Online]. Available: https://resolver.caltech.edu/CaltechAUTHORS:20140808-104301806

[10] P.-H. Yeh, K.-A. Chang, J. Henriksen, B. Edge, P. Chang, A. Silver, and A. Vargas, "Large-scale laboratory experiment on erosion of sand beds by moving circular vertical jets," Ocean Engineering, vol. 36, no. 3, pp. 248–255, 2009. [Online]. Available: https://www.sciencedirect.com/science/article/pii/S0029801808002473

[11] G. Chiaia, A. Petrillo, and G. Ranieri, "Erosion of Loose Beds by Submerged Circulair Impinging Vertical Turbulent Jets," Journal of Hydraulic Research, vol. 35, no. 4, pp. 567–574, Jul. 1997, publisher: Taylor & Francis _eprint: https://doi.org/10.1080/00221689709498412. [Online]. Available: https://doi.org/10.1080/00221689709498412

[12] C. Dong, G. Yu, H. Zhang, and M. Zhang, "Scouring by submerged steady water jet vertically impinging on a cohesive bed," Ocean Engineering, vol. 196, p. 106781, Jan. 2020. [Online]. Available: https://linkinghub.elsevier.com/retrieve/pii/S0029801819308819

[13] B. Westrich and H. Kobus, "Erosion of a uniform sand bed by continuous and pulsating jets," PROC. 15TH CONGRESS IAHR (ISTANBUL), vol. 1, no. (Sep.3-7, 1973), pp. 91–98, 1973.

[14] S. Zhang, C. Wang, and T. Ge, "Experimental prediction of the noncontact jet Trencher's excavation depth in clay," Marine Georesources & Geotechnology, vol. 35, no. 2, pp. 300–304, Feb. 2017, publisher: Taylor & Francis _eprint: https://doi.org/10.1080/1064119X.2016.1149530. [Online]. Available: https://doi.org/10.1080/1064119X.2016.1149530

[15] W. Mih and J. Kabir, "Impingement of water jets on nonuniform streambed," Journal of Hydraulic Engineering, vol. 109, no. 4, pp. 536–548, 1983.

[16] X. Yan, A. Mohammadian, and C. D. Rennie, "Numerical modeling of local scour due to submerged wall jets using a strict vertex-based, terrain conformal, moving-mesh technique in OpenFOAM," International Journal of Sediment Research, vol. 35, no. 3, pp. 237–248, Jun. 2020. [Online]. Available: https://www.sciencedirect.com/science/article/pii/S1001627920300019

[17] G. Franz, P. Leitão, L. Pinto, E. Jauch, L. Fernandes, and R. Neves, "Development and validation of a morphological model for multiple sediment classes," International Journal of Sediment Research, vol. 32, no. 4, pp. 585–596, 2017.

[18] T. Wang and B. Song, "Study on deepwater conductor jet excavation mechanism in cohesive soil," Applied Ocean Research, vol. 82, pp. 225–235, Jan. 2019. [Online]. Available: https://www.sciencedirect.com/science/article/pii/S0141118718303535

[19] B. Wang, C. van Rhee, A. Nobel, and G. Keetels, "Modeling the hydraulic excavation of cohesive soil by a moving vertical jet," Ocean Engineering, vol. 227, p. 108796, 2021. [Online]. Available: https://www.sciencedirect.com/science/article/pii/S0029801821002316

[20] M. Constant, F. Dubois, J. Lambrechts, and V. Legat, "Implementation of an unresolved stabilised FEM–DEM model to solve immersed granular flows," Computational Particle Mechanics, vol. 6, no. 2, pp. 213–226, Apr. 2019. [Online]. Available: https://doi.org/10.1007/s40571-018-0209-4

[21] "Gmsh: a three-dimensional finite element mesh generator with built-in pre- and post-processing facilities." [Online]. Available: https://gmsh.info/

[22] R. J. LeVeque, Numerical methods for conservation laws, 2nd ed., ser. Lectures in mathematics ETH Zürich. Basel ; Boston: Birkhäuser Verlag, 1992.

[23] J.-F. Remacle and G. Winckelmans, "Equations aux dérivées partielles, lfsab1103 mathématiques 3."

[24] "CHAPTER 2 - Flow Drilling: Underbalance Drilling with Liquid Single-Phase Systems," in Underbalanced Drilling: Limits and Extremes, B. Rehm, A. Haghshenas, A. Paknejad, A. Al-Yami, J. Hughes, and J. Schubert, Eds. Gulf Publishing Company, Jan. 2012, pp. 39–108. [Online]. Available: https://www.sciencedirect.com/science/article/pii/B9781933762050500097

UNIVERSITÉ CATHOLIQUE DE LOUVAIN
École polytechnique de Louvain
Rue Archimède, 1 bte L6.11.01, 1348 Louvain-la-Neuve, Belgique | **www.uclouvain.be/epl**